



Evolution of micro-damage and degradation of macro-mechanical properties of sandstone due to thermal effects

Pin Wang^{1,2} · Tubing Yin¹ · Xibing Li¹ · Heinz Konietzky²

Received: 23 June 2021 / Accepted: 2 February 2023 / Published online: 21 February 2023
© Springer-Verlag GmbH Germany, part of Springer Nature 2023

Abstract

Previous studies on thermal induced damage of rocks concentrated mainly on the analysis of macro-mechanical properties. This paper documents physical and microstructural characteristics of sandstone after high-temperature treatment by using several testing methods at the micro scale. Results indicate that physical including mechanical parameters of tested sandstone show some strengthening effect up to a temperature of about 100 °C, which is related to the evaporation of free water and the thermal expansion of mineral particles. Beyond 100 °C, the physico-mechanical properties of sandstone are weakened significantly. Mass loss and porosity show a continuously growing with increasing temperature, while P-wave velocity, splitting tensile strength, compression strength, and elastic modulus are decreasing. Nuclear magnetic resonance (NMR) imaging tests were carried out to capture the variations in porosity and pore size distribution characteristics of sandstone during the heat treatment. With increasing temperature, the number of macropores and microcracks increase and coalesce. There is a linear relationship between rock porosity and tensile as well as compressive strength. Differential thermal analysis (DTA) shows that the α - β phase transition of quartz minerals occurs at a temperature of 573.4 °C. Additionally, between 400 and 600 °C, more transgranular microcracks are observed detected by optical microscope and scanning electron microscopy (SEM) observations, which proves that quartz phase transition is an important factor to induce microcracks. Thermal treatment also has a significant influence on the variation of the brittle index of sandstone, which makes thermal-induced plastic deformations of the sandstone more obvious.

Keywords Sandstone · Thermal damage · Pore structure characteristics · Microscopic mechanisms

Introduction

The influence of temperature on strength, deformation, and stability of rock masses has become an important scientific problem in the field of rock mechanics and engineering (Brotóns et al. 2013; Tian et al. 2014). With the development of geothermal energy generation, oil exploitation, nuclear waste storage, and the utilization of deep underground space, research on the characteristics of rocks and bedrock at elevated temperatures is becoming more and more important (Yi et al. 2019; Shafiei and Dusseault 2013; Liu et al. 2014; Wood and Kaewsomwang 2018). Additionally, deep rock mass

engineering is often affected by sudden high-temperature jumps such as explosion or fire. Post-disaster reconstruction, repair, reinforcement, as well as safety assessments also need to consider changes in the mechanical behaviour of the rock after potentially subjected to high temperature (Hajpál 2002; Chakrabarti et al. 1996). Therefore, the influence of temperature changes on the mechanical properties of rocks is an important factor that cannot be ignored when studying the problems of deep rock engineering.

Rock as a natural geological material is a mixture of various mineral particles and pores. Rocks contain many defects such as non-uniform distribution of joints and cracks. These defects play a vital role for the macroscopic deformation of rocks under mechanical and thermal loading and lead to inhomogeneous, anisotropic, and inelastic behaviour (Zhao et al. 2019; Braun et al. 2019). Over the last decades, substantial effort has been made to explore the thermal effects on various rock types regarding physical and mechanical properties. For example, Tian et al. (2012) systematically

✉ Tubing Yin
tubing_yin@mail.csu.edu.cn

¹ School of Resources and Safety Engineering, Central South University, Changsha 410083, China

² Geotechnical Institute, TU Bergakademie Freiberg, Freiberg 09596, Germany

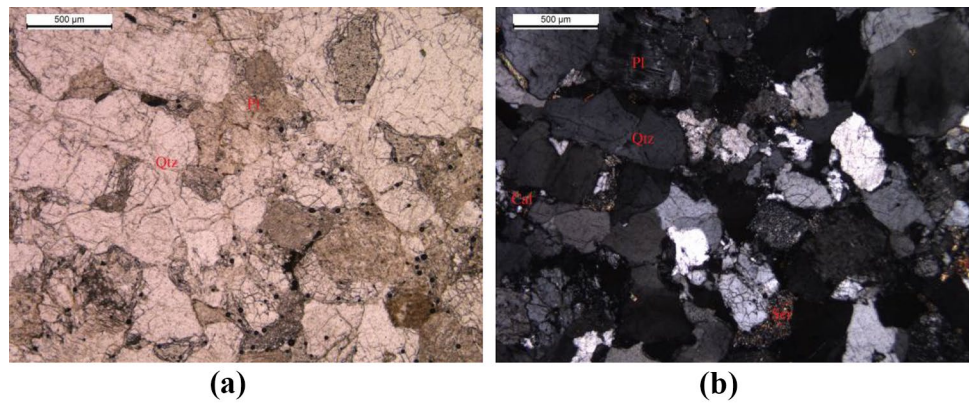
reviewed the effect of high temperature on the physical properties (including bulk density, porosity, permeability, and compressional wave velocity) of sandstone based on an extensive literature study. They reported that changes in the physical properties of sandstones are too small to be neglected after heat treatments at 100–200 °C but usually decline significantly above 400 or 500 °C treatment. Li et al. (2020) studied the changes in pore structure and mechanical properties of sandstone after high-temperature treatment using nuclear magnetic resonance. They observed that high temperatures significantly increased the porosity and permeability of the sandstone and that the compressive strength continued to decrease with increasing temperature. Lü et al. (2017) carried out Brazilian tests on the Linyi sandstone at temperatures ranging from 25 to 900 °C. They found that the indirect tensile strength and longitudinal wave velocity of the sandstone decreased with increasing temperature over the entire temperature range tested. Brotóns et al. (2013) studied the physical and mechanical properties of a porous rock (San Julian's calcarenite) heated up to 600 °C that involved UCS tests with two different cooling methods. Their results showed that the compressive strength and elastic modulus decrease proportionally to the temperature and that the thermal weakening effect greatly depends on the cooling method. It can be generalized from the studies mentioned above that temperature usually causes significant "thermal damage" to rocks, weakening their strength and physical properties. However, studies have also indicated that rock strength may not necessarily decrease with increasing temperature. Ranjith et al. (2012) carried out uniaxial compression tests on the Hawkesbury sandstone at various temperatures from 25 to 900 °C. They reported that the compressive strength and elastic modulus of the sandstone increased with increasing temperature before 500 °C, whereas the opposite variations were observed for temperatures greater than 500 °C. Rao et al. (2007) investigated the mechanical properties such as the indirect tensile strength, compressive strength, elastic modulus, and mode I fracture toughness of thermally treated sandstone. They observed that these mechanical parameters are linearly increased with the increasing temperature below a specific temperature of 200 or 250 °C. Mahanta et al. (2016) further studied the influence of thermal treatment on the mode I fracture toughness of three kinds of Indian rocks. Test results indicated that fracture toughness decreased progressively with increasing temperature, but all these rocks showed varying degrees of increase in fracture toughness up to a temperature of 100 °C. They stated that the increase in fracture toughness might be related to the evaporation of free water and the closure of pre-existing fractures within the rock.

In summary, current research on the thermal damage of rocks mainly focuses on the macroscopic physical and

mechanical properties. Due to the significant difference in different rock types, rock-forming conditions, and mineral compositions, various microscopic damage mechanisms have been put forward for rock weakening by high temperatures, including thermal expansion (Sirdesai et al. 2019; Meng et al. 2020), thermal cracking (Fredrich and Wong 1986; Griffiths et al. 2018; Wong et al. 2021; Zuo et al. 2018), water release (Wong et al. 2020; Tian et al. 2014), phase transition (Glover et al. 1995; Wang et al. 2019; Zhang et al. 2021), decomposition (Liu et al. 2019), melting (Ersoy et al. 2021; Tripathi et al. 2021), recrystallization (Wadsworth et al. 2016), and dehydroxylation (Funatsu et al. 2004; Mollo et al. 2011; Heap et al. 2012). To reveal the underlying mechanisms of temperature effects on rock strength, many scholars have also studied the physical characteristics of rocks during the destruction process considering electromagnetic radiation (Vostretsov et al. 2010), acoustic emission (Rong et al. 2018; Li et al. 2018), micro-seismicity (He et al. 2011), and infrared thermal radiation (Ma and Zhang 2019). However, the internal structure of rocks experience complex changes under high temperature and extreme loads. The development of microcracks and pores caused by changes in the internal stress field under extreme temperature as well as changes in the mineral composition and structure caused by physical and chemical reactions can have a significant impact on the mechanical behaviour of rocks (Liu et al. 2016, 2019; Meng et al. 2020). Therefore, it is necessary to carry out an in-depth study of the mineralogical and microstructural characteristics of rocks exposed to different high temperatures, which will be helpful in accurate predictions of rock stability in engineering applications.

The aim of this study is to reveal the underlying mechanisms of temperature influence on rock strength. The effect of temperature on the physical and mechanical properties of sandstone was first analysed. Temperature-induced microscopic damage was then investigated through an integrated approach involving petrographic thin section analysis, scanning electron microscopy (SEM) observation, X-ray diffraction (XRD), and differential thermal analysis (DTA). On this basis, relationships between the microscopic failure mechanisms and the macroscopic mechanical characteristics for sandstone exposed to high temperature are deduced. To better understand the damage process and mechanisms, the results of this study were compared with previously published literature on different types of sandstone. The results suggested that the mismatch in thermal expansion of the mineral grains and their chemical decomposition at different temperatures are the main reasons for the deterioration in rock strength. Additionally, the mechanical properties of sandstones containing more clay minerals are more likely to be strengthened by temperature.

Fig. 1 Micrographs of the Changsha sandstone obtained by optical microscope under **a** plane and **b** cross-polarized light (Qtz, quartz; Pl, plagioclase; Cal, calcite; Ser, sericite)



Materials and methods

Sample preparation

In this study, the fine-grained sandstone collected from Changsha city (Hunan province, China) was selected for experiments due to its isotropic and homogeneous. The surface colour is greyish-white with a certain light green at room temperature. Microstructure and mineralogical characteristics of sandstone were studied by optical microscope (Fig. 1). The X-ray diffraction technique is used to determine the mineral composition of the sandstone, and the specific mineral content in weight percentages are quartz (65.68 wt%), feldspar (21.35 wt%), montmorillonite (4.58 wt%), muscovite (3.67 wt%), and chlorite (4.72 wt%), as listed in Table 1.

To eliminate the effects of anisotropy, all sandstone samples are drilled from a single rock block in the same direction and prepared according to the recommendation of the International Society of Rock Mechanics (ISRM) (Zhou et al. 2012; Bieniawski and Hawkes 1978). The diameter of the samples was about 50 mm, and two different length/diameter ratios were processed, 2.0 and 0.5 for the uniaxial compression and indirect tension tests, respectively. The circumference and end surfaces of the samples were polished to ensure that the non-parallelism of the end surface is less than 0.02°, and the surface unevenness is less than 0.02 mm. For further analysis, samples with similar density and P-wave velocity were selected to minimize the influence of rock inhomogeneity. The bulk density and P-wave velocity of the dry samples was approximately 2.59 g/cm³ and 3247 m/s, respectively. In addition, the average value of the total

porosity of the tested sandstone specimens (before thermal treatment) is about 3.21%, determined by using the nuclear magnetic resonance (NMR) tests, as shown in Fig. 2.

On the other hand, we further measured the porosity of sandstone specimens before high-temperature treatment using a conventional mercury intrusion porosimetry (MIP) method. The test results are shown in Fig. 3. It could be observed from Fig. 3 that the cumulative pore volume increases slowly along with the pressure before closing to 100 psia. However, when the pressure exceeds 100 psia, the cumulative pore volume correspondingly increases rapidly. Furthermore, if the pressure is higher than 3000 psia, the cumulative pore volume nearly keeps constant. In the mercury ejection curve, the cumulative pore volume remains constant when the pressure is higher than 1000 psia but declines as the pressure decreases to 1000 psia below. In addition, the porosity of the sandstone specimens obtained using the MIP method is smaller than that measured by the NMR test; they were approximately 3.07% and 3.21%, respectively. The main reason for this discrepancy is that many rock samples, especially low-porosity and low-permeability rock samples, are less than 100% saturated with piezometric mercury, while the NMR technique can detect very small pores in rock samples, which also proves that the NMR technique has its unique advantages in measuring small pores and complex pore distribution.

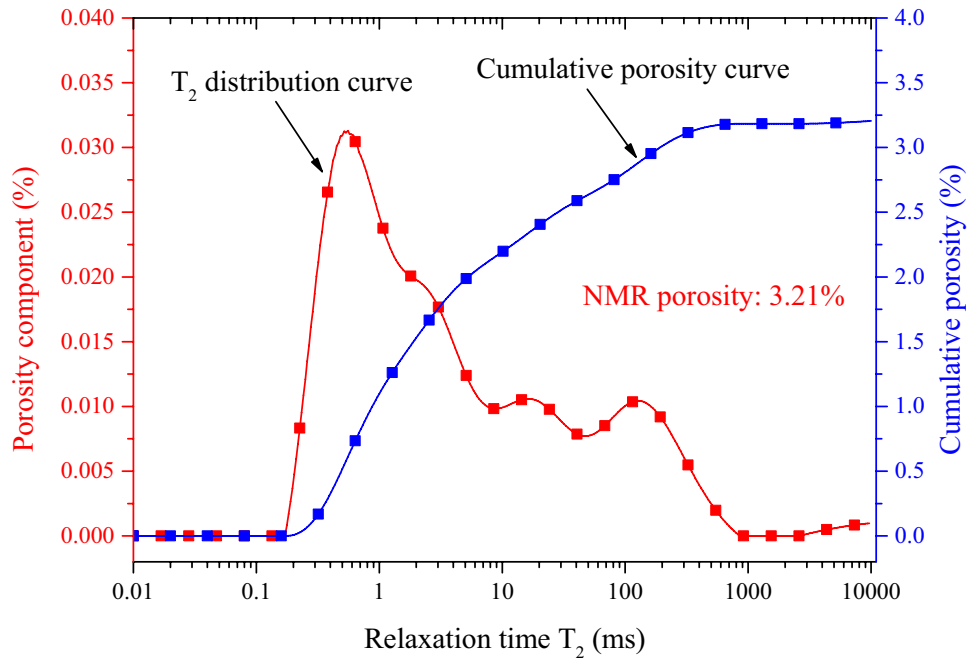
Experimental setup and procedure

The experimental technique and test procedures are given in Fig. 4. It can be divided into four sections: sample

Table 1 Summary of the main mineral composition of Changsha sandstone

Mineral composition	Chemical formula	Grain radius (mm)	Content (wt%)
Quartz	SiO ₂	0.25–0.6	65.68
Feldspar	KAlSi ₃ O ₈ , NaAlSi ₃ O ₈ , CaAl ₂ Si ₂ O ₈	0.4–0.6	21.35
Montmorillonite	(Na, Ca) _{0.33} (Al, Mg) ₂ [Si ₄ O ₁₀](OH) ₂ ·nH ₂ O	0.1–0.2	4.58
Muscovite	KAl ₂ (AlSi ₃ O ₁₀)(OH) ₂	0.06–0.3	3.67
Chlorite	(Mg, Fe) ₅ (Al, Fe) ₂ Si ₃ O ₁₀ (OH) ₈	0.08–1.2	4.72

Fig. 2 NMR T_2 distribution curve and porosity calculation of sandstone at room temperature

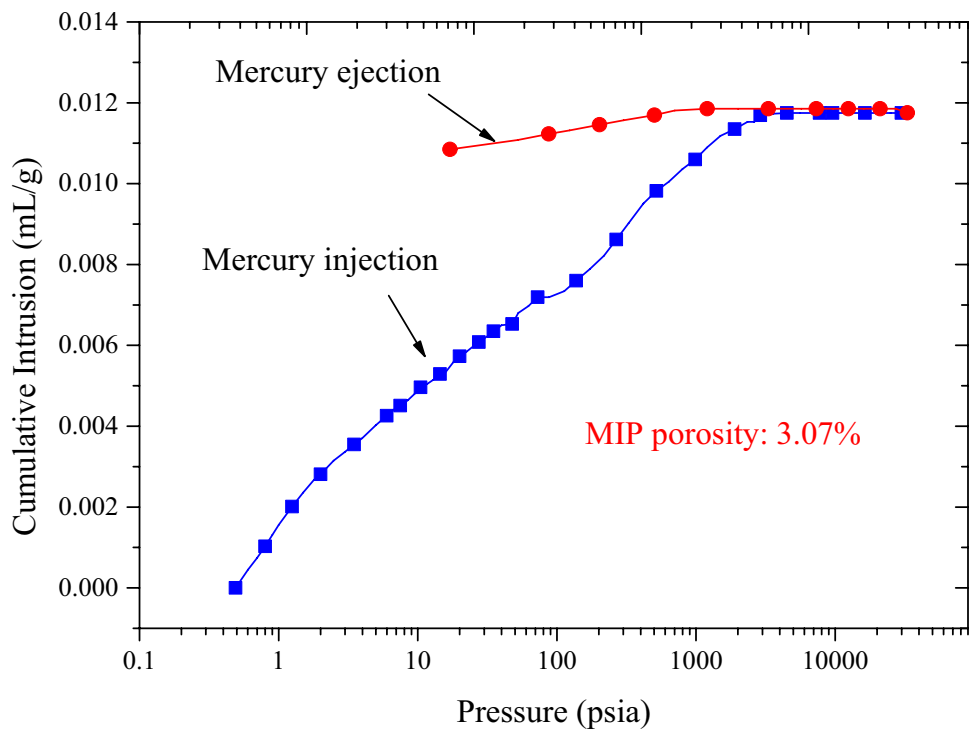


heating process, measurement of physical parameters, mechanical strength tests, and mineralogical and microstructural analyses. The detailed test procedure and setting parameters are as follows:

- (I) Sample heating process: the thermal treatment of sandstone was conducted in a high-temperature box-type resistance furnace (muffle furnace), shown

in Fig. 4a. The maximum heating temperature of the furnace is 1300 °C, and the heating rate can be servo-controlled. For this study, the temperature was set to eight levels: room temperature (25 °C) and 100, 200, 400, 600, 800, 1000, and 1200 °C, with seven specimens in each group (six samples were used for mechanical testing and the other one for mineralogical analysis). The heating process was

Fig. 3 The porosity of sandstone calculated by a conventional mercury intrusion porosimetry (MIP) method



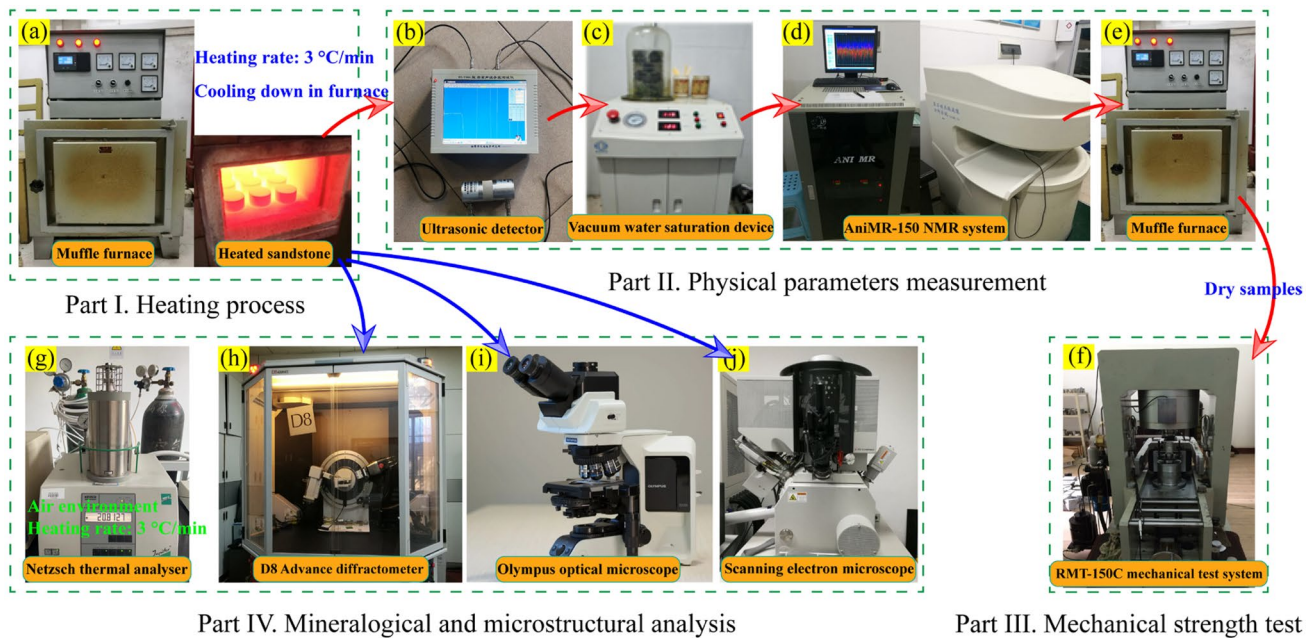


Fig. 4 Experimental system and test procedure

carried out with 3 °C/min until the specified temperature was reached, and then the temperature was kept constant for 2 h to ensure that the temperature is uniform inside the sample. Thereafter, samples are naturally cooled down to room temperature in the furnace to avoid thermal shock damage caused by the temperature difference between the heating furnace and outside environment (Shen et al. 2020; Nasseri et al. 2009). After completion of the heat treatment, all specimens were placed in a drying oven at room temperature (around 25 °C) for the experiments of the next stage.

- (II) Measurement of physical parameters: after completion of the thermal treatment, some basic physical parameters of all sandstone samples will be first measured, including weight, volume, bulk density, P-wave velocity, and porosity. The variation in bulk density can be calculated from the tested weight and volume of samples. P-wave velocity was determined using an HS-YS4A ultrasonic detector, and the measurement process was carried out according to the suggested method by ISRM (Aydin 2014). During the test, the ultrasonic transducer is aligned with the centre of the two ends of the sample, and petroleum jelly is used as a coupling agent to maintain a good coupling between the transducer and the tested sandstone surface, shown in Fig. 4b. Regarding the porosity measurement, a low-field AniMR-150 NMR testing system was adopted in our work, as shown in Fig. 4d. It should be noted

that the NMR method focuses on obtaining the pore structure and porosity of rocks by measuring the relaxation properties of hydrogen-containing nuclear fluids inside the rock. Since natural rocks rarely contain fluids, NMR tests can hardly detect any electromagnetic signals on dry rocks. Additionally, the water saturation degree of the rock plays a significant effect in the porosity measurement results. Therefore, rock samples must be treated in a vacuum water saturation device (Fig. 4c) for more than 48 h to reach a fully saturated state. The theory of low-field NMR techniques will be described in detail in the next section.

- (III) Mechanical strength test: before mechanical strength testing, all sandstone samples were dried in a muffle furnace at 105 °C for about 24 h, as shown in Fig. 4e. After that, the uniaxial compression and Brazilian disc tests on dry sandstone samples were carried out on an RMT150C hydraulic servo testing machine, as shown in Fig. 4f. The loading capacity of this machine can be up to 2000 kN, and the testing system can record vertical loads and displacement. For the Brazilian disc test, the sandstone disc was compressed diametrically under force-controlled loading by a flat load platen without any cushion strips or loading jaws on the specimen. A constant loading rate of 0.02 kN/s was selected for the compression and indirect tension tests.
- (IV) Mineralogical and microstructural analysis: in terms of thermal analysis, the mass loss and heat

exchange of sandstone minerals due to chemical and physical reactions were measured with a simultaneous thermal analyser (NETZSCH Instruments Co., STA 449C) at a heating rate of 3 °C/min, between 25 and 1200 °C, under an air atmosphere, showed in Fig. 4g. In addition, the mineral fractions of sandstone specimens subjected to different high temperatures were analysed using the powder compact method on a D8-Advance X-ray diffractometer, shown in Fig. 4h. To reveal the variation in microstructural characteristics of sandstone, optical thin-section microscopic observation and scanning electron microscopic analysis were also carried out on sandstone samples after exposure to different high temperatures, shown in Fig. 4i and j.

Theory of low-field NMR techniques

Nuclear magnetic resonance (NMR) is used to measure the porosity of sandstone, which is based on the magnetic properties of atomic nuclei and their interaction with the applied magnetic field. It mainly measures the relaxation characteristics of the hydrogen-containing nuclear fluid in the rock pores. When a water-saturated sandstone is put into a constant magnetic field, the application of the radio frequency (RF) field will cause the hydrogen nuclei to resonate and absorb RF pulse energy. When the RF field is removed, the absorbed RF energy will be released by the hydrogen nuclei. The process of the energy release can be detected through a special coil, and a signal whose amplitude is attenuated

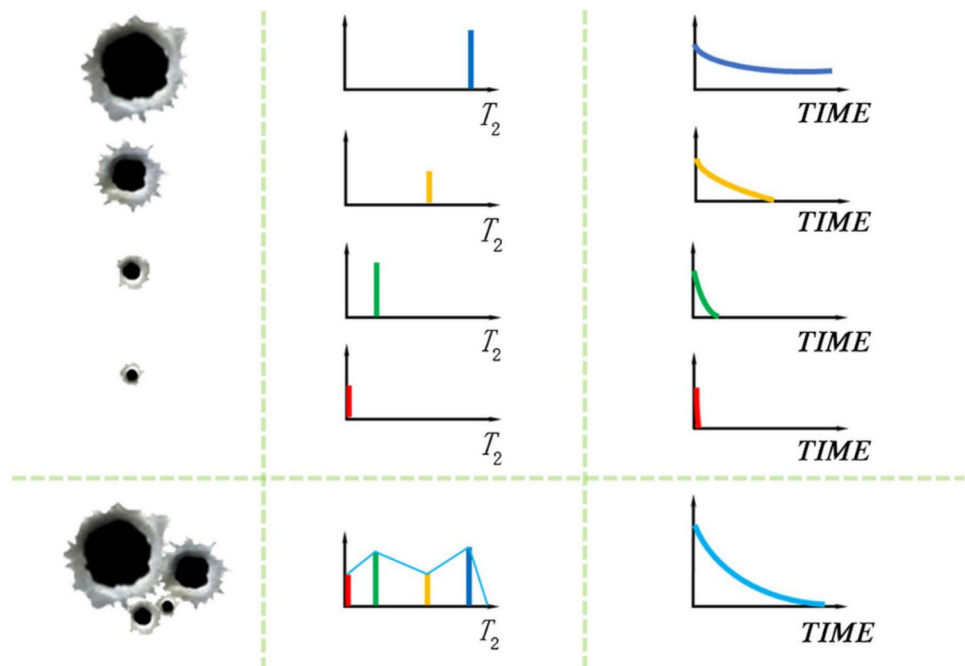
exponentially with time can be received, which is the nuclear magnetic resonance signal (Li et al. 2016). As the rock skeleton does not generate magnetic resonance signals when the specimen is fully saturated, pore water distribution characteristics measured by NMR can truly reflect the pore structure characteristic of the sandstone.

In addition, for samples with different properties, the energy release rate is different. The pore structure of the rock usually has a pore size distribution, and each pore size has its own characteristic relaxation time T_2 . By analysing the distribution difference of the T_2 curve, a change in rock pore structure can be detected. Figure 5 shows the multi-exponential relaxation decay curve in porous media (Xue et al. 2018).

The pores on the left side in Fig. 5 represent the size and number of pores within the sample being tested. In NMR testing, the size of the pore diameter within the rock corresponds to the position of the different diffraction peaks on the X-axis, and the diversity of pore diameters determines the number of diffraction peaks in the T_2 distribution curve. According to the distribution characteristics of the peaks of the multi-exponential relaxation decay curve T_2 shown in Fig. 5, the pore aperture can be observed. The larger the pore size of the rock, the longer the corresponding relaxation time, and the stronger the shift of the T_2 distribution curve to the right. The relationship between pore size and relaxation time T_2 can be expressed as (Yao et al. 2010; Jin et al. 2020).

$$\frac{1}{T_2} = \rho_2 \frac{S}{V} \quad (1)$$

Fig. 5 Multi-exponential relaxation decay curve T_2 in porous media (Xue et al. 2018)



where T_2 is the relaxation time (s) of pore fluid caused by surface relaxation, ρ_2 is the relaxation strength of surface fluid (m/s), S is the surface area of the pore (m^2), and V is the volume of pore fluid (m^3).

Results and discussion

Physical properties of heated sandstone

Colour changes and surface cracks of the sandstone after different high-temperature treatments are shown in Fig. 6. The colour of the specimens of the Changsha sandstone selected for this study was greyish-white with a certain light green at room temperature. The surface of the samples is flat and clean, with no obvious defects observable by the naked eye. After high-temperature treatments at 100–200 °C, the sandstone mainly underwent dehydration of free water, and there was almost no significant change in surface colour and volume. After treatment at 400–600 °C, the surface colour of the sample gradually changed from greyish-white to red or light yellow, and the light green on the surface of the samples gradually disappeared. The typical chemical reaction caused by heating is the oxidation of iron in the calcium matrix, which leads to a change in colour from light green to red (Gautam et al. 2016; Hajpál and Török 2004).

Above 800 °C, morphological changes became more obvious, and the volume expanded significantly. When the temperature was further increased to 1000 °C, some mineral grains underwent a considerable degree of expansion, the surface of the sample became rough due to loosening of mineral particles, and some obvious macroscopic cracks appeared. When the temperature exceeded 1200 °C, the surface colour of the sandstone sample changed from yellow to black, and some transparent crystals appeared on the surface. This phenomenon might be caused by the melting of the aluminosilicate

in the sandstone (Sirdesai et al. 2019; Zhang et al. 2017). The sandstone specimens experienced high-temperature metamorphism, and the overall structure changed. Some of them were severely damaged and lost almost their bearing capacity. Therefore, samples treated at 1200 °C were not used subsequent mechanical testing.

Figure 7 documents that the density of tested sandstone generally decreases linearly after high-temperature treatment compared to room temperature. However, the mass loss after high-temperature treatment did not show a linear increase but showed a parabolic relation (growth rate gradually slowed down). There might be two reasons for the variation of sandstone density after thermal treatment: at low temperature, the heat treatment causes internal water loss, and the reduction in weight during this stage is the leading factor causing the decrease in density. However, as the treatment temperature increases, the internal moisture of the sandstone is completely lost. Even at higher temperature, the mass variation caused by the thermal decomposition of mineral components is relatively small, and as a result, the weight remains nearly constant. However, increasing temperature causes mineral expansion, increasing volume, and consequently decreasing density. Mass loss and change in density of the sandstone as function of temperature follow the relationships (regression analysis):

$$\xi(T) = 3.95 - 4.38e^{-T/241.38} \quad (R^2 = 0.99) \quad (2)$$

$$\rho(T) = 2576.57 - 0.188T \quad (R^2 = 0.98) \quad (3)$$

where $\xi(T)$ and $\rho(T)$ stand for mass loss and density of the sandstone samples after heating at temperature T .

The acoustic parameters affected by temperature are important for analysing the occurrence and development of internal microcracks in heat-treated rocks, and they are also useful to study the physical and mechanical properties of the rock (Liu and Xu 2015). In this study, the ultrasonic

Fig. 6 Surface colour changes and crack evolution in sandstone after high-temperature treatment

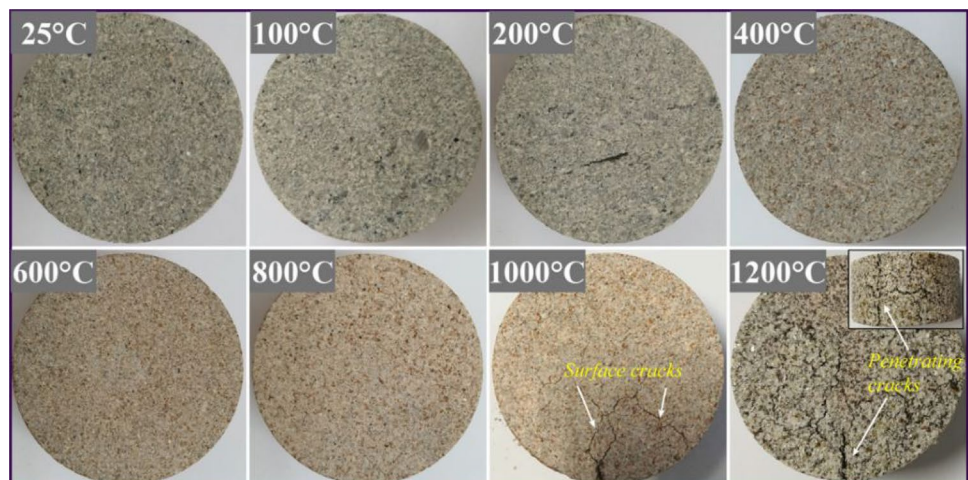
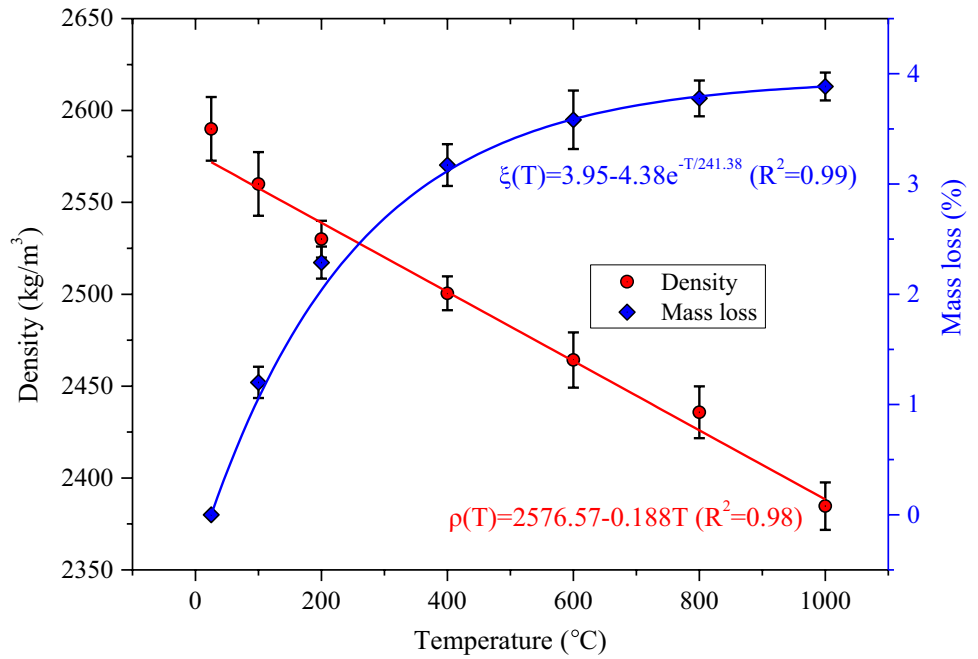


Fig. 7 Rock density and mass loss vs. temperature (mean value and standard deviation)

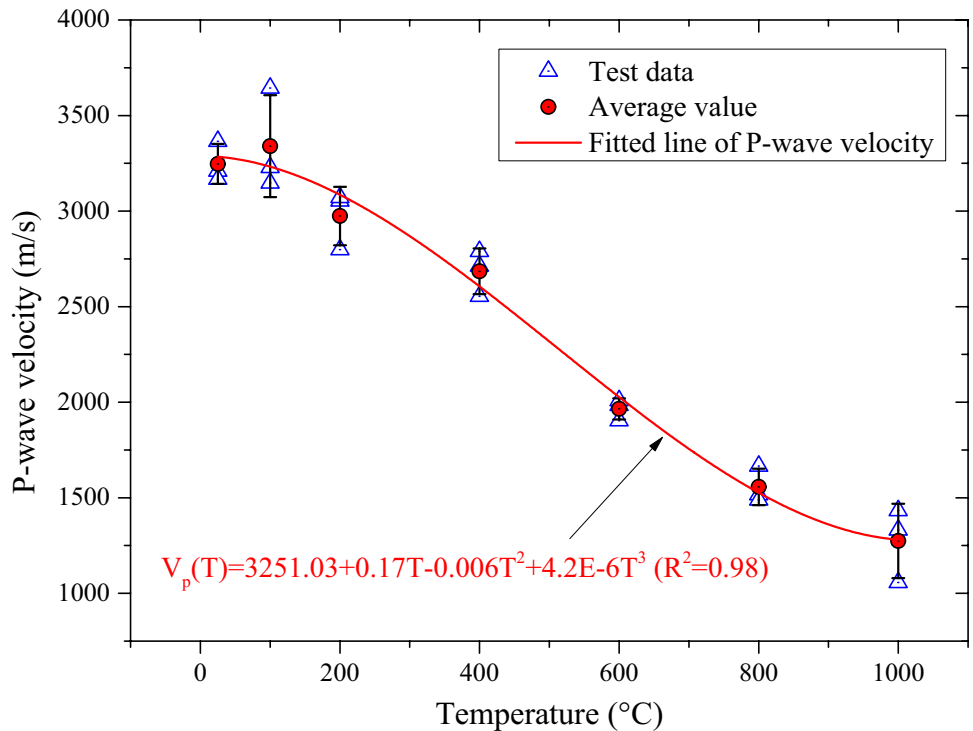


P-wave velocity of all sandstone samples before and after high-temperature heating was measured (Fig. 8).

Figure 8 shows that P-wave velocity increases up to about 100 °C. The main factor contributing to this phenomenon is the closure of pre-existing microvoids and microcracks within the rock due to the thermal expansion of mineral particles, increasing the compactness of the

sandstone. When temperature exceeds 100 °C, the P-wave velocity continuously decreases with increasing temperature, indicating that the high temperature has caused obvious thermal damage to the sandstone. On the one hand, under the influence of high temperature, the evaporation of free water forms water vapour, which causes an increase in pore volume and hinders the propagation of ultrasonic

Fig. 8 P-wave velocity vs. temperature (mean value and standard deviation)



waves to some extent; on the other hand, the uneven expansion of different minerals at high temperature leads to induced thermal stresses, which leads to development and expansion of microcracks and micro holes in the rock, but also to stronger attenuation of the ultrasonic wave energy. The following equation describes the relationship between P-wave velocity and temperature:

$$V_p = 3251.03 + 0.17T - 0.006T^2 - 4.2e^{-6}T^3 \quad (R^2 = 0.98) \quad (4)$$

NMR T₂ spectrum distribution and pore characteristics

The T₂ spectrum of sandstone samples after treatment at different temperatures is shown in Fig. 9a. Peak position and area of the T₂ spectrum represent size and corresponding number of pores, and the curve represents the distribution

pores in terms of size (Frosch et al. 2000). In this study, the NMR T₂ spectrum of the sandstone sample shows 3 peaks at around 0.5 ms, 1 ms, and 80 ms. The abscissa positions of these three relaxation peaks are similar, which indicates that the pore size distribution of sandstone has not changed substantially up to 1000 °C.

In the temperature range between 25 and 200 °C, the peak value of the first relaxation peak does not change much. However, when the temperature exceeds 200 °C, the first peak value decreases first and then increases, which is related to the expansion of rock particles and the initiation of new microcracks at higher temperature. Additionally, with increasing temperature, the positions of the three relaxation peaks of the T₂ curve gradually move away from the coordinate origin, which indicates that the average diameter of the pores is increasing under high temperature.

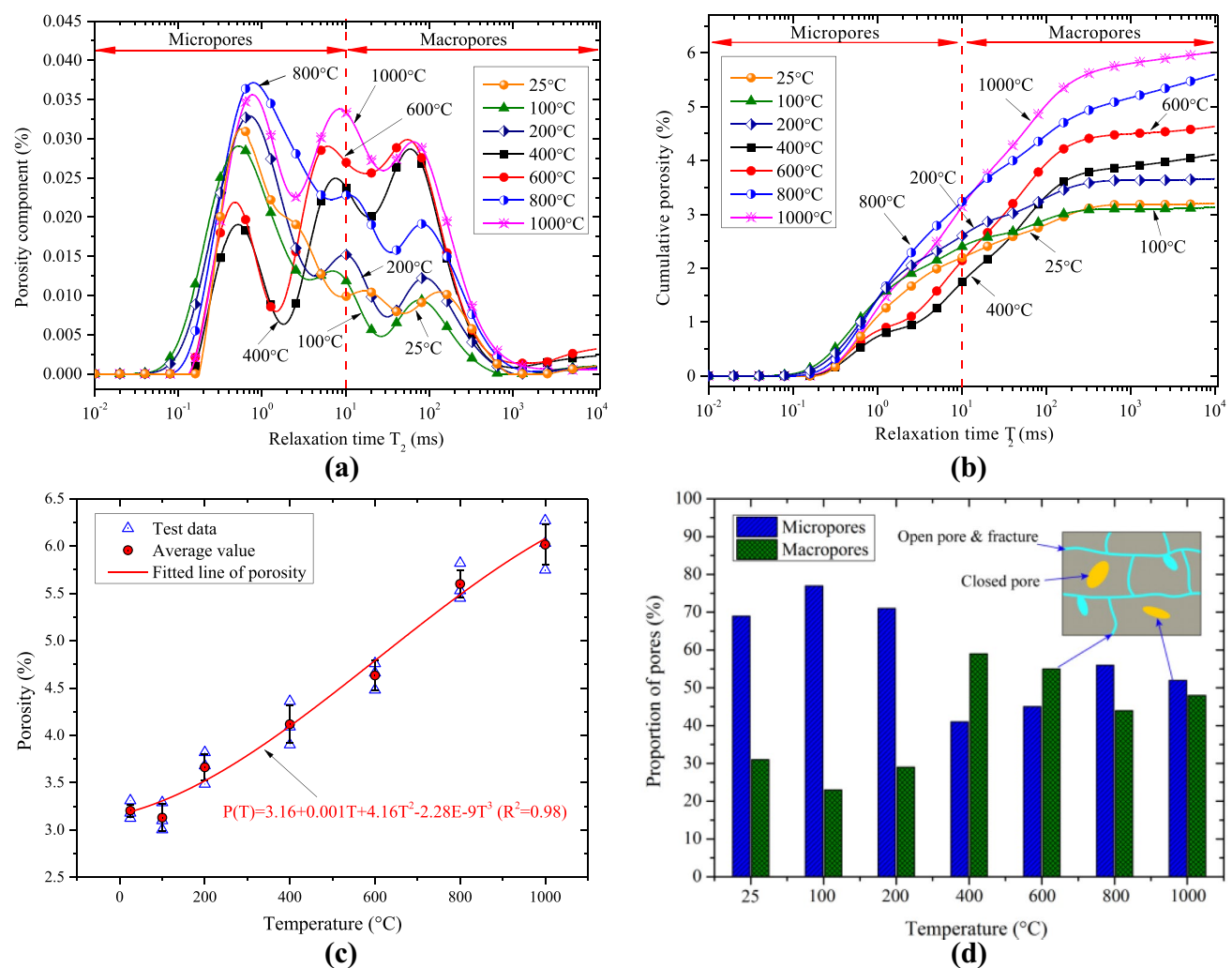


Fig. 9 NMR test results and the pore structure characteristics of sandstone after different high-temperature treatments: **a** T₂ spectrum of sandstone specimens; **b** curves of cumulative porosity of sandstone

specimens; **c** curves of variation of rock porosity with increasing temperature; **d** proportions of micropores and macropores in the specimens

Figure 9b shows the relationship between cumulative porosity and relaxation time for sandstone after treatment at different high temperatures. The variation of porosity after treatment was calculated as shown in Fig. 9c. By regression analysis, rock porosity and temperature meet the following equation:

$$P(T) = 3.16 + 0.001T + 4.16T^2 - 2.28e^{-9}T^3 \quad (R^2 = 0.98) \quad (5)$$

Figure 9c documents that porosity exhibits a completely opposite trend in comparison to the P-wave velocity (see Fig. 8). At 100 °C, the rock porosity is slightly decreased, suggesting that the thermal expansion of minerals particles and the closure of pre-existing microcracks have produced a more compact rock, which leads to “negative” damage.

Many scholars have studied the consistency between nuclear magnetic resonance and mercury intrusion method in respect to the estimation of the pore structure and believe that the T_2 cut-off line can be used to segment the T_2 spectrum of saturated rocks, for instance, into bound pores and free pores (Coates et al. 1999; Westphal et al. 2005). The bound pores and free pores also indicate the closed and open states of pores in the rock, respectively (Yao et al. 2010). The bound water generally exhibits a shorter T_2 relaxation time, and the movable water has a longer T_2 relaxation time. Therefore, T_2 cut-off value is a key parameter to discriminate the form of movable and bound water and then to evaluate pore structure and pore size distribution. According to Li et al. (2015) and Tang et al. (2016), for rock or coal masses, the average T_2 cut-off is 10 ms. A value of $T_2 < 10$ ms corresponds to micropores that are filled with bound water, and a value of $T_2 > 10$ ms corresponds to macropores or microcracks from which the water can be easily drained. Therefore, this paper also uses 10 ms as the T_2 cut-off line to further analyse the pore size distribution of the sandstone as shown in Fig. 9a and b.

Figure 9d shows that the proportion of micropores and macropores in sandstone changes obviously with increasing temperature. In the temperature range between 25 and 200 °C, the proportion of micropores in sandstone is higher, but with increasing temperature, the number of micropores decreases, and the proportion of macropores increases. When the temperature is between 400 and 600 °C, the number of macropores exceeds the number of micropores. When the temperature continues to rise, the proportions of macropores and micropores become approximately equal.

The distribution of hydrogen nuclei (^1H) in the water-saturated rocks can be obtained with the help of magnetic resonance imaging (MRI) technology; generally, the MRI signal can be visualized as a grayscale image. Because water has difficulty penetrating the rock matrix, grayscale images of water-saturated rocks can reveal the distribution of pores and microcracks in damaged rock specimens. Since the grayscale value depends on the density of the ^1H , it is easy to

surmise that the larger the pores and cracks, the higher the density of the ^1H , the higher the grayscale value, and the brighter the pixels. To improve the recognizability of the MRI images, we converted the grayscale images into proton density-weighted photos according to the grayscale values of the pixels, as shown in Fig. 10. On the colour bar, a high proton density (light) denotes a relatively high moisture content (Xie et al. 2018). From 25 to 100 °C, the main colour of the NMR images is blue, the bright spots are evenly distributed, and some areas are darker. This indicates that the number of pores in this section is small, the distribution is uniform, and most of the pores are of small size. When the temperature rises to 200 °C, the area of the blue bright spots increases gradually, which indicates that the temperature has caused damage and deterioration of the sandstone, increasing the number of micropores and microcracks and further enlarging the size of primary microcracks.

When the temperature reaches 400 °C, the blue areas continue to increase and brighten, and some green aggregation areas appear in some regions. The damage effect of temperature is further strengthened, and microcracks gradually converge in the rock and coalesce, forming larger microcracks, thus providing more channels for the entry of water. During the 600 to 1000 °C phase, more penetration and aggregation is observed (indicated by green areas). The bright and white areas in the MRI results become larger and larger, which indicates that a large number of intergranular and transgranular microcracks have been produced, and the length and width of the microcracks gradually increased. It is noteworthy that some minerals in sandstone melt and recrystallize when the treatment temperature rises to 1200 °C, resulting in redistribution of the pore structure and a reduction of the overall porosity during recrystallization, and some larger bubbly pores are produced in some local areas.

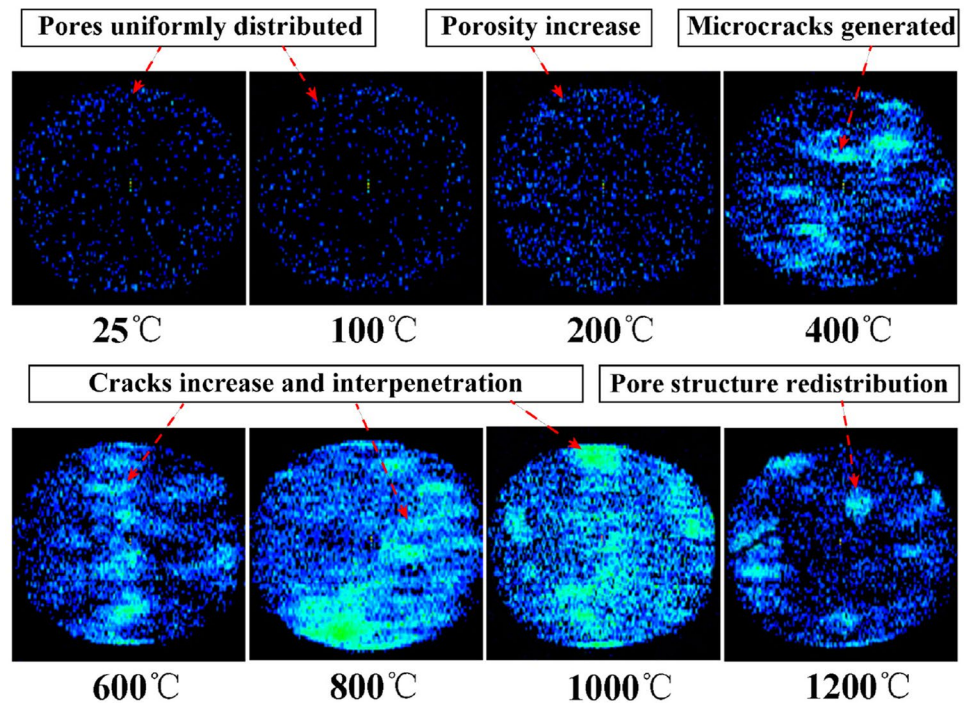
Strength and elastic modulus

Compressive stress–strain curves and tensile load–displacement curves of sandstone exposed to different temperatures are shown in Fig. 11a and b.

The stress–strain curves of specimens treated before at different temperatures are not linear but reveal an obvious microcrack compaction process. Generally speaking, the higher the treatment temperature was, the longer the stage of closure of primary microcracks. This is consistent with the previous results of NMR imaging. Therefore, high temperature increases the porosity of the rocks, so the crack and pore closure stage becomes longer.

Figure 12 shows the temperature dependence of compressive strength, tensile strength, and elastic modulus of sandstone after different high-temperature treatments. In this study, the elastic modulus is determined by the slopes corresponding to 40% and 60% of the compressive strength in the rising stage of

Fig. 10 MRI results of cross-sections of samples subjected to different temperature



the stress–strain curve. The graphs illustrate that uniaxial compressive strength, indirect tensile strength, and elastic modulus of sandstone in general decrease with increasing temperature, but all three mechanical parameters show an exception up to the temperature of about 100 °C. The main reasons for this phenomenon may be related to the increased inter-particle friction due to the evaporation of pore water and the closure of pre-existing microcracks due to the thermal expansion of mineral grains. Under the combined effect of these two factors, the compactness and strength of the sandstone are enhanced.

However, with increasing temperature, the uneven expansion of different minerals at higher temperature leads to an increase in thermal stresses; consequently more microcracks are generated, which result in strength decrease. Figure 13 gives the relation between rock porosity and mechanical strength, which indicates a good linear relationship between rock porosity and strength. It can be concluded that thermal treatment changes the porosity characteristics and initiates micro mechanical damage of the rock, which is the main reason for its mechanical property degradation. Based on a regression analysis, the following

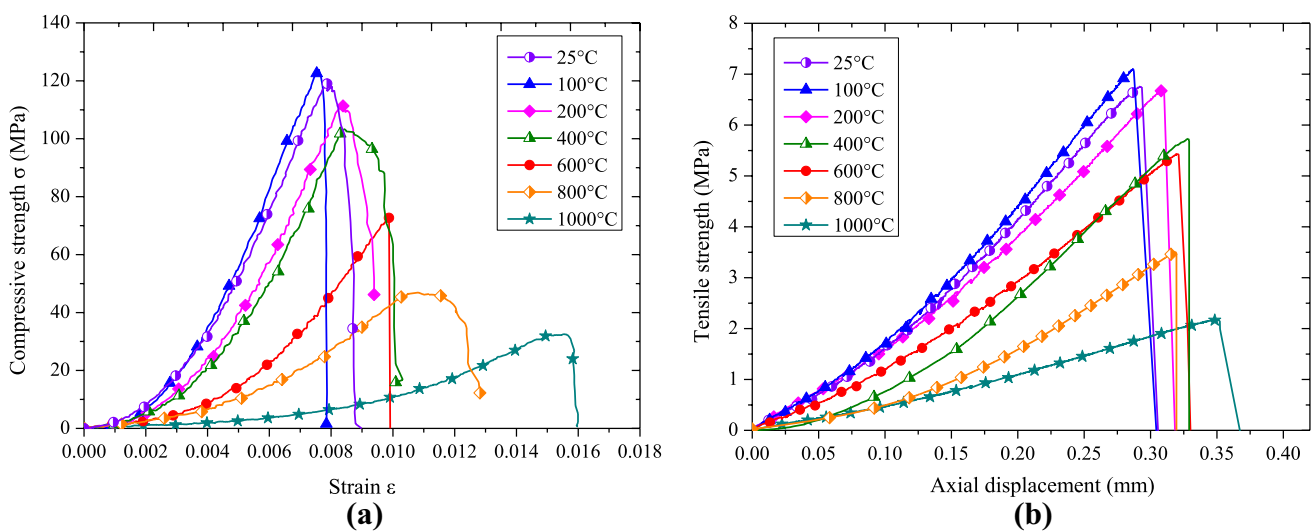


Fig. 11 Mechanical test results of sandstone after different temperature treatments: **a** uniaxial compressive stress–strain curves; **b** axial load–displacement curves obtained from Brazilian tests

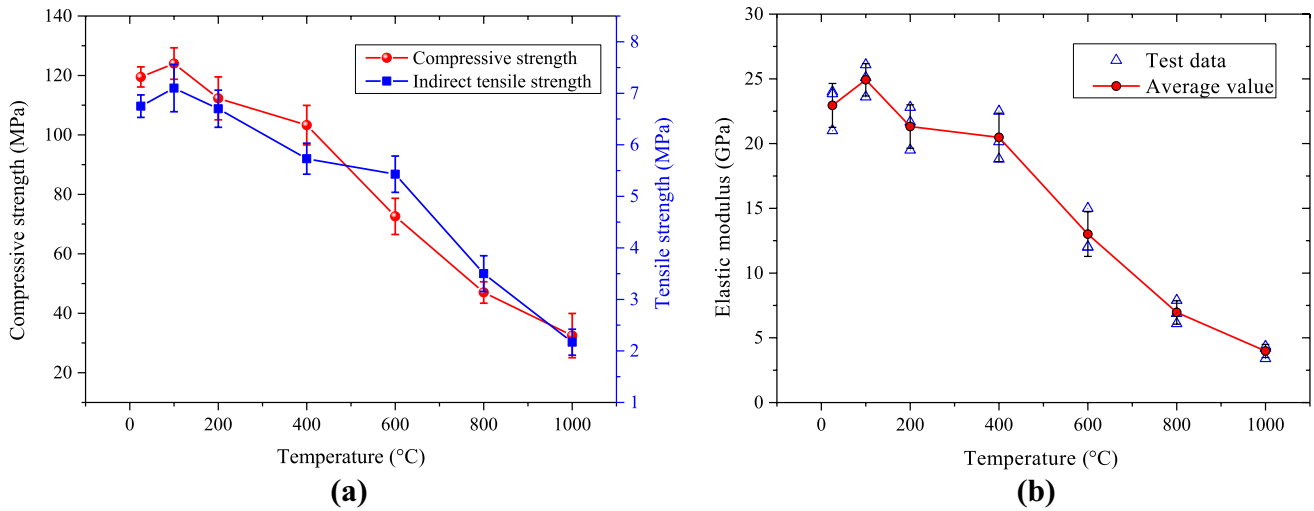


Fig. 12 Rock strength (a) and elastic modulus (b) vs. temperature (mean value and standard deviation)

relations are obtained for the uniaxial compressive strength (UCS) and the Brazilian tensile strength (TS):

$$UCS = 226.47 - 32.08P \quad (R^2 = 0.98) \quad (6)$$

$$TS = 12.26 - 1.59P \quad (R^2 = 0.95) \quad (7)$$

Beyond a temperature of about 400 °C, the elastic modulus decreases rapidly, which might be closely related to the brittleness characteristics. In order to quantify this finding, the relationship between the brittleness index (defined as ratio between tensile and compressive strength) and temperature is presented (Altindag 2010) as shown in Fig. 14. The brittle index shows a significant drop at a temperature between 400 and 600 °C, which is also reflected by the behaviour of the elastic modulus. The main reason for this

sharp decline of the brittle index of sandstone is the comprehensive effect of the development of transgranular microcracks and the thermoplastic deformation of some minerals after high-temperature treatment (Ranjith et al. 2012). More details on the intrinsic mechanisms which are responsible for the brittle index decline in rocks at high temperatures will be discussed in the following sections.

Thermal effects and evolution of micro-damage

Thermal expansion and cracking mechanisms

The internal energy of rocks increases gradually under the action of high temperature, resulting in thermal expansion of mineral components. Due to the different thermal

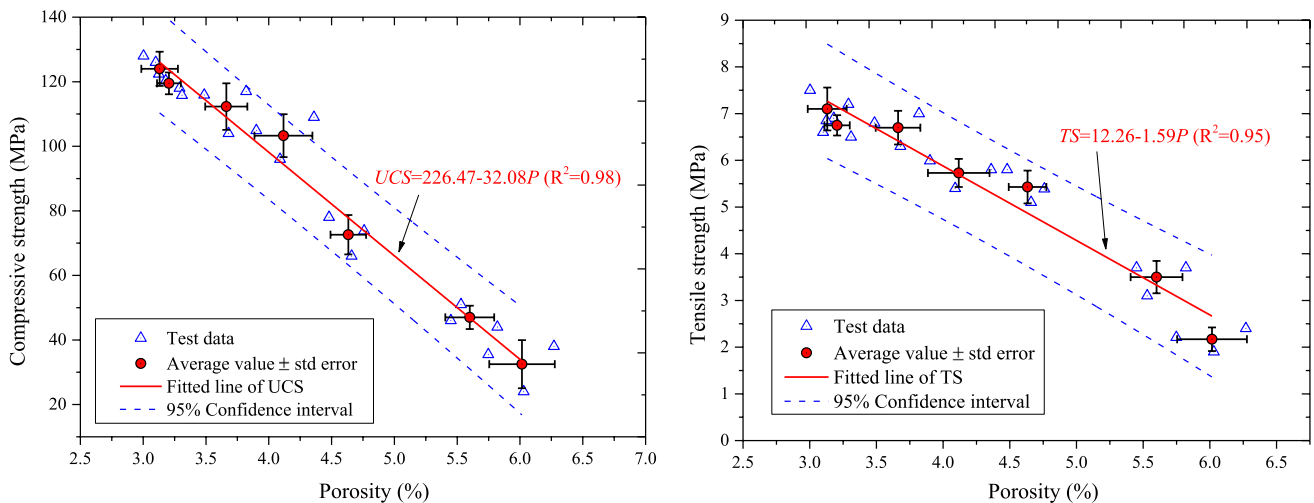


Fig. 13 Rock strength vs. porosity (mean value and standard deviation)

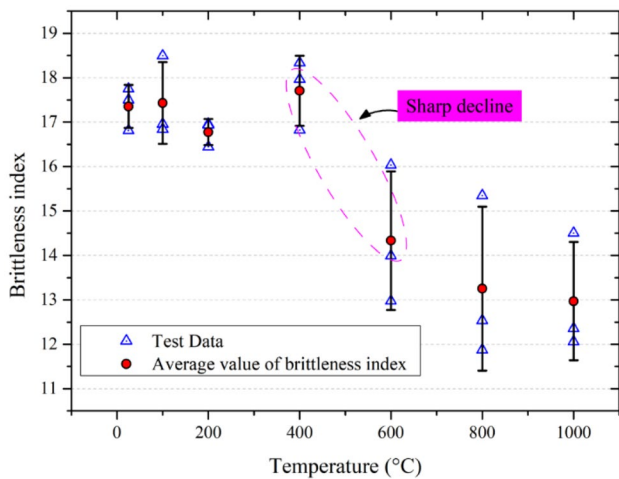


Fig. 14 Brittleness index vs. temperature (mean value and standard deviation)

expansion coefficients and anisotropy of different mineral particles, a local concentration of thermal stresses occur at the particle contacts.

Figure 15 shows optical electron microscopy images of sandstone specimens exposed to different temperatures (25–1200 °C). The images are magnified by a factor of 10. It becomes visible that at room temperature, there are more intergranular microcracks in the sandstone, and the connectivity between the cracks is better. When the temperature rises to 100 °C, mineral particles touch each other more closely, and some primary microcracks are closed. When the temperature reaches 200 °C, the width of intergranular microcracks increases, and some new intergranular microcracks gradually develop. When the temperature reaches 400 °C, the surface of the crystals has become very rough, intergranular microcracks have developed, and transgranular microcracks are forming (presumed to be caused by uneven deformation of mineral particles, resulting in thermal stress of the structure). Between 600 and 800 °C, the microscopic pictures change significantly, intergranular microcracks and transgranular microcracks are well developed, and voids between particles have increased, which is presumed to be caused by the melting of fillers or some minerals. When

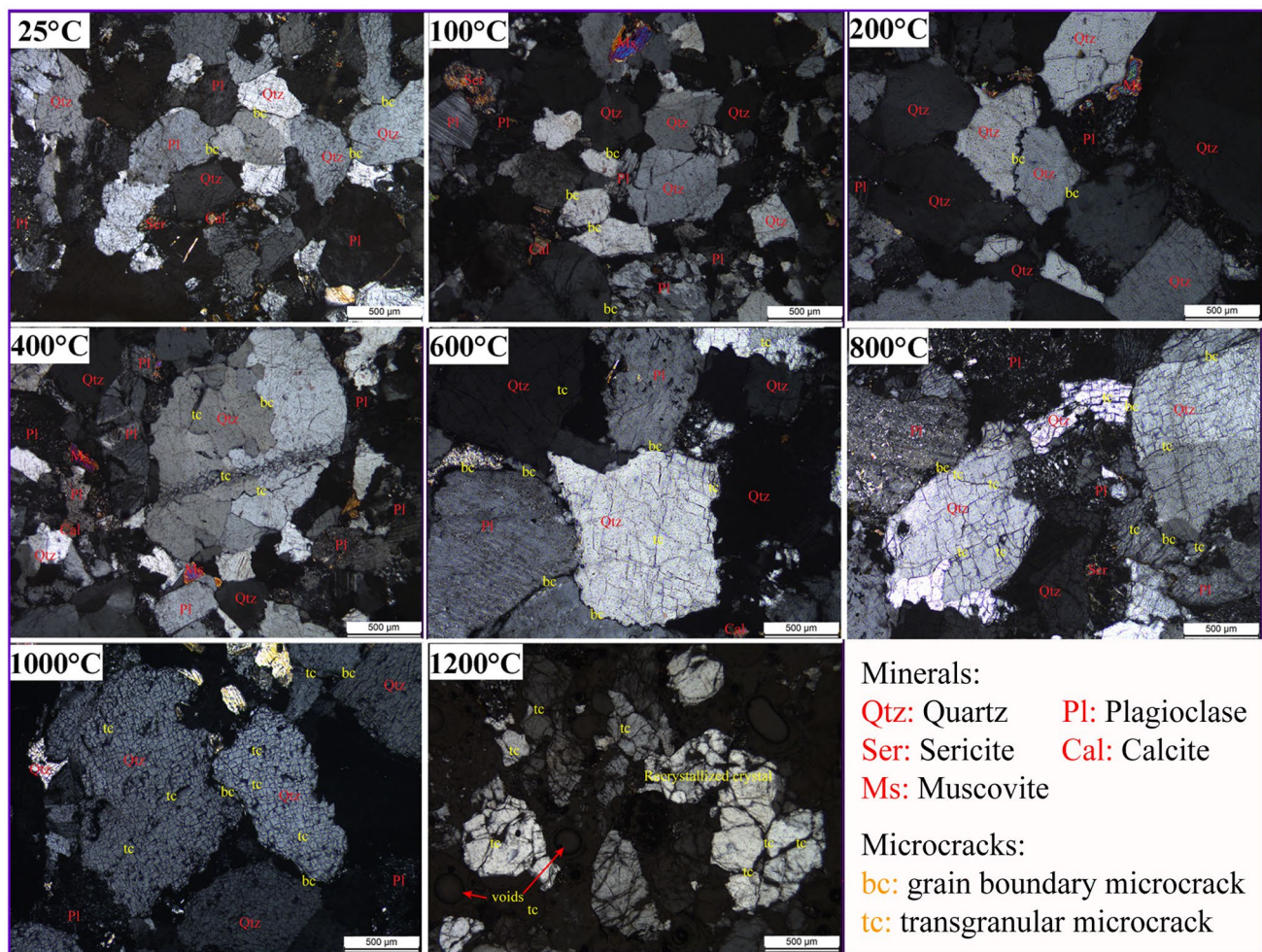


Fig. 15 Optical microscopic images of sandstone specimens after different high-temperature treatments

the temperature reaches 1000 °C, the sandstone crystals are gradually damaged by transgranular microcracks, and the integrity of the crystal structure is obviously damaged. When the temperature rises to 1200 °C, uncrystallized rocks have fewer micro-fissures but many holes due to the melting of some mineral particles.

In order to clarify the effect of the average thermal deformation of mineral particles at different temperature on microcrack growth, the average particle size of mineral particles after exposure to different high temperatures was counted by arranging measuring lines under optical and electronic microscopes. The thermal deformation parameters of mineral particles after exposure to high temperature are shown in Fig. 16. It can be inferred that below about 600 °C, with increasing temperature, the size of mineral particles increases approximately linear and continuously. Therefore, it can be concluded that below about 600 °C, the formation of new microcracks in rocks can be mainly attributed to the structural thermal stress caused by the non-uniform deformation of mineral particles. However, when the temperature exceeds about 600 °C, the crystal particles show a downward trend, and at 1000 °C, the thermal deformation becomes negative. The main reason for this phenomenon is the melting and transgranular microcracks of the crystals, which results in a large reduction in the average particle size. Especially after high-temperature treatment at 600 °C, a large number of transgranular microcracks were found within the quartz mineral grains. It can be concluded that the quartz phase transition might be one of the important factors leading to the significant reduction of sandstone grain size.

Mineralogical changes due to heat

For each mineral, the lattice type, the number of atoms in the cell, the position of atoms, and the size of the cell are

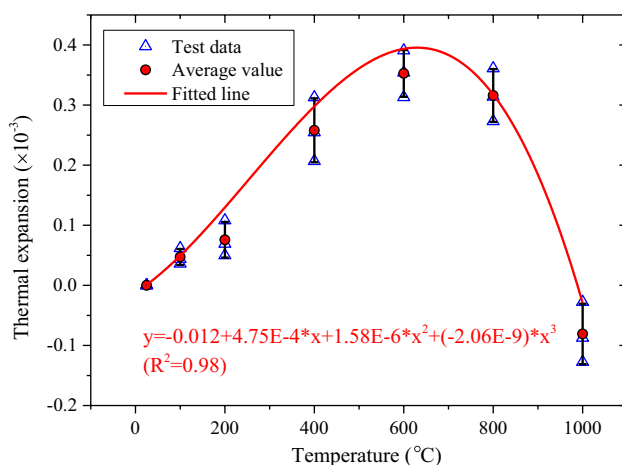


Fig. 16 Thermal expansion of the average particle size vs. temperature (mean value and standard deviation)

specific. Under the condition of heat treatment, the periodicity of mineral crystals will be destroyed to some extent, resulting in additional phase differences and changes in the diffraction intensity of minerals. By comparing the XRD information and the content of rock minerals after different temperature treatments as shown in Fig. 17a and b, it is found that the most significant change is that the diffraction peaks of some minerals disappear after heat treatment. For example, the diffraction peaks of muscovite and chlorite disappear after treatment at 800 °C, and the diffraction peaks of montmorillonite and feldspar minerals decrease sharply after treatment at 1200 °C. However, quartz minerals are relatively stable, and no disappearance of the diffraction peaks is observed in the temperature range between 25 and 1000 °C, but the diffraction intensity differs after treatment at different temperatures. When the temperature rises to 1200 °C, the diffraction peaks of cristobalite appear. Very similar results were also reported by Wadsworth et al. (2016). These phenomena indicate that some thermal reactions must occur in sandstone at different stages of high-temperature treatment.

Furthermore, the physicochemical reactions of sandstone during exposure to high temperature were studied by using differential scanning calorimeter (DSC) and thermal gravity (TG) analysis in an air environment (Fig. 18). It can be observed that the DSC curve of sandstone shows a trough at about 151.5 °C and two further troughs at about 573.4 and 701.5 °C, indicating that endothermic reactions have taken place. We can conclude that the first trough at a temperature of 151.5 °C is caused by evaporation of free water in the rock, because the TG curve is significantly reduced by 1.19% in the temperature range from 25 to 200 °C. In addition, the XRD results show that there is no disappearance of the diffraction peaks of rock minerals below 600 °C, and although the endothermic process of rocks occurs at the peak of 573.4 °C, it does not cause a decrease of the TG curve, so it can be inferred that the α - β phase transformation of quartz minerals occurs in this stage (Lider and Yurtseven 2018; Karunadasa et al. 2018).

With regard to the third trough of the DSC curve at 701.5 °C, the corresponding TG curve shows a significant weight loss, indicating that there is a decomposition reaction of minerals. This mass loss corresponds to the fact that there are many water-bearing minerals in the sandstone, such as montmorillonite, muscovite, and chlorite (as evidenced by Liu et al. 2016 and Chen et al. 2017). In these water-bearing minerals, water can be divided into two major types, namely intergranular water and crystalline water. As intergranular water is not involved in the crystalline composition of the mineral, its loss temperature is generally low. However, as the treatment temperature increases, the crystalline water is gradually removed from the mineral particles, resulting in the destruction of the crystal structure of minerals through dehydration. Such

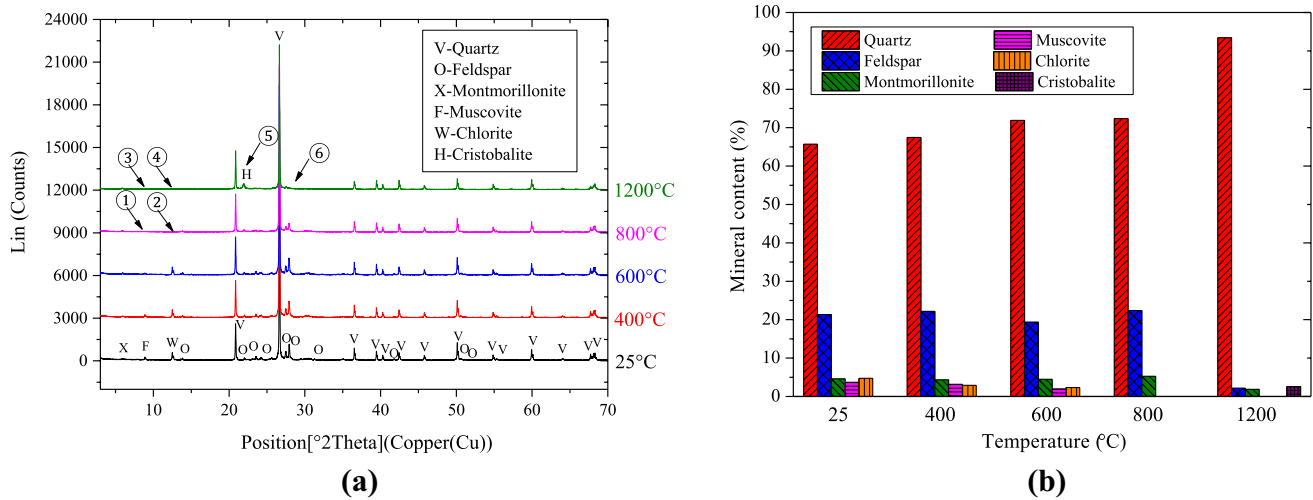


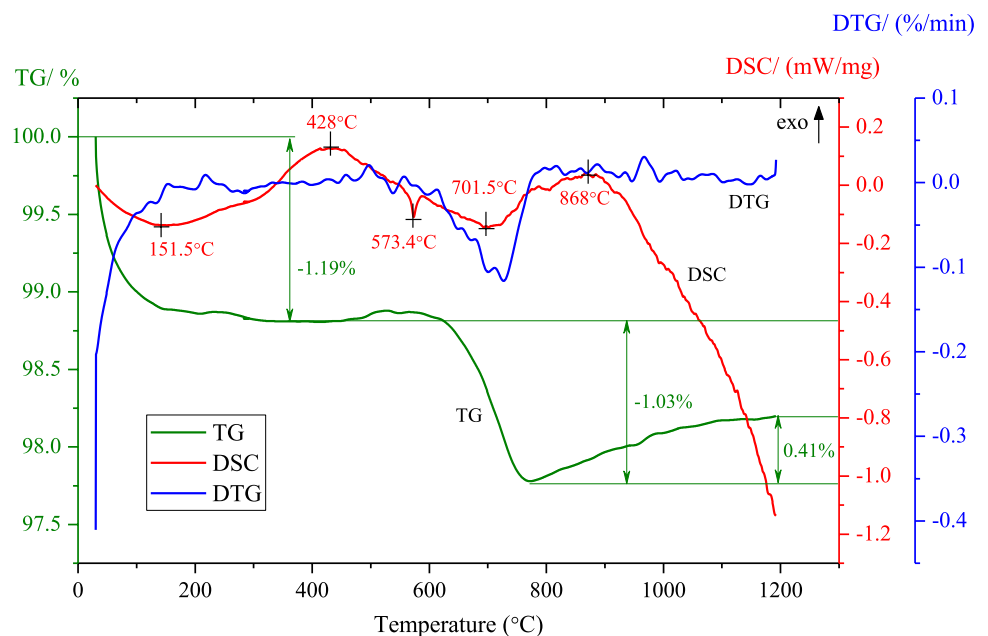
Fig. 17 XRD analysis (a) and mineral content vs. temperature (b)

a reaction is also called dehydroxylation (Funatsu et al. 2004; Mollo et al. 2011; Heap et al. 2012). Therefore, it can be concluded that the diffraction peaks of muscovite and chlorite disappear after treatment at 800 °C is mainly caused by the dehydroxylation effect. However, it should be noted that the diffraction peaks of the montmorillonite minerals did not disappear after the high-temperature treatment at 800 °C, which may be related to the crystal structure of the minerals and the higher temperature of dehydroxylation (Wu et al. 1999; Lin et al. 1999; Wolters and Emmerich 2007).

In addition, it should be noted that there are two exothermic valleys at the temperature of 428 and 868 °C, which

indicates that some oxidation reactions take place. For the first exothermic valley, there is evidence that this is caused by the oxidation of ferrous ion (Zhang et al. 2019), which is also a good explanation for the apparent reddening of the rock surface (see Fig. 6) after thermal treatment with 400 °C. For the second exothermic valley, a marked increase in the TG curve is observed, which may be related to the absorption of water or some gases in the air during the oxidation of rock minerals. On the other hand, when the temperature rises to 1200 °C, the DSC curve shows a sharp decrease. Combining these results with the XRD test results, it can be seen that the melting of feldspar minerals occurs in this stage. On the other hand, because the α - β quartz phase transition

Fig. 18 TG, DSC, and DTG curves of Changsha sandstone



is irreversible under the action of the high temperature of 1200 °C, high-cristobalite content is found in the diffraction pattern (see Fig. 17a).

Microcrack evolution under external stress

Microscopic morphology analysis is an important tool to study the rock microstructure. To some extent, the structural failure characteristics in the process of damage evolution can be inferred from the microscopic fracture morphology. Fracture evolution includes stages of microcrack initiation and propagation and coalescence, and many deformation marks are left on the microcrack morphology in each stage.

In the temperature interval between 25 and 200 °C, some obvious intergranular microcrack firstly appeared (Fig. 19). In this stage, the strength of interstitial fillings determines the failure strength of the rock. When the temperature rises to 400 °C, transgranular microcracks occurs in the sandstone, and the microcrack spacing is large. Under external load, the crystal strength begins to play an increasingly important role. When the temperature rises to 600–800 °C, slip separation and dimples occur in the interior of the rock. Slip separation and dimples are the two most common morphological features for ductile rock fractures. It also indicates that after experiencing a high temperature of 600–800 °C, the rock shows more likely plastic deformation and fractures. When the temperature increases to 1000 °C, the crystal particles become loosened, and the fractured surfaces become rough, forming a crushed zone.

Some minerals in sandstone are melted after thermal treatment of 1200 °C, which results in a very loose structure and significantly reduced load-bearing capacity. Therefore, no additional mechanical tests have been carried out on it.

But SEM-based microstructure observations were also carried out as shown in Fig. 20a and b. It could be observed that the internal structure has changed fundamentally after experiencing extreme high temperature: no obvious crystal grain boundaries and numerous pores can be found any more. With the help of X-ray energy-dispersive spectrometer (EDS), quantitative analysis of element mass fraction considering original (point 002) and molten minerals (point 001) was conducted (Fig. 20b).

Results listed in Table 2 show that the content of silicon in recrystallized minerals is significantly lower than in unmelted minerals. Although the phase transition of quartz minerals is irreversible beyond 1200 °C, it is just a structural change, and the content of silicon is not changed significantly (Glover et al. 1995). Additionally, the content of sodium and aluminium in recrystallized minerals is higher than that in unmelted minerals. Therefore, it can be concluded that melting and recrystallization of aluminosilicates in rocks might be the main causes (feldspar minerals are involved in them). This result also provides evidence for the rapid decline of the DSC curve beyond a temperature of 1000–1200 °C.

Comparison with existing literature

In most cases, the exposure of rocks to high temperatures will lead to a significant reduction in their physical and mechanical properties. However, the influence of temperature on the mechanical properties of rock is complicated by the diversity of mineral composition, the type of cementation, and the development of internal micro defects—different kinds of rock show different mechanical responses under the influence

Fig. 19 SEM observations of fracture morphology of sandstone after thermal treatments

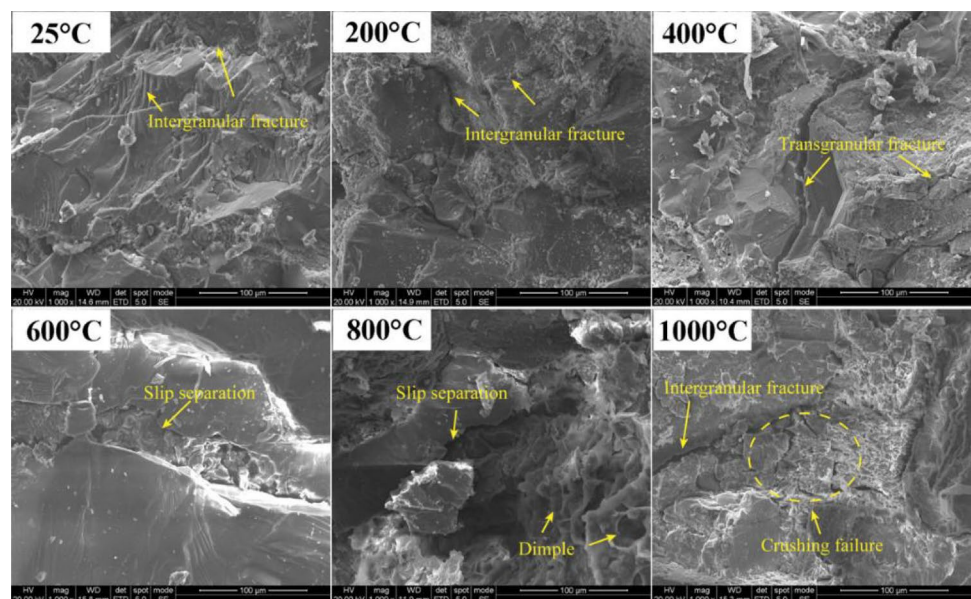
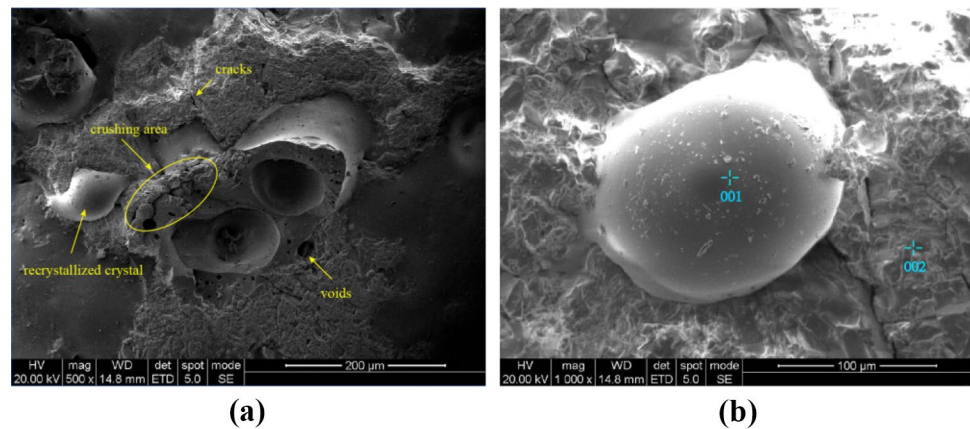


Fig. 20 SEM observations (a) and EDS quantitative analysis (b) of melted sandstone experienced temperature of 1200 °C



of temperature. Even if the same type of rock is affected by temperature, there are significant differences in the changes in mechanical properties. Table 3 summarizes the experimental data from previously published literature concerning the physical and mechanical properties of sandstone after exposure to different high temperatures, and the results from our study have been compared with them, shown in Fig. 21. It could be observed from Fig. 21a and b that the variation in normalized UCS and BTS of the sandstone with temperature can be divided into four different stages.

In the first stage (0–200 °C), the normalized values of UCS and BTS show an increasing trend in the first stage as the temperature rises. For the normalized UCS, our data agree well with the experimental results of Zhang et al. (2016). Since the physicochemical properties of the rock-forming minerals are relatively stable until 100 or 200 °C, the only reliable explanation is that the expansion of the mineral grains causes the pore space inside the rock to be compacted (Wong et al. 2020). The most direct evidence of this is the reduction in porosity of the sandstone in this study at 100 °C, shown in Fig. 9c. In addition, Wong et al. (2020) suggested that the increased friction between mineral grains due to pore water loss is also an important cause of the increased strength of the rock. In contrast, Li et al. (2020) and Hajpál and Török (1998) reported that the compressive strength of the sandstone continues to decrease during this stage. The main reason for this difference may be related to the porosity of the rock. For low porosity sandstones, the expansion and deformation of the mineral particles are restricted. Under the combined effect of thermal expansion mismatch and structural thermal stress, microcracks generate within the sandstone, reducing its strength.

In the second stage (200–400 °C), as the temperature rises, some of the main minerals of the sandstone, such as quartz and mica, undergo more significant volume expansion (Tripathi et al. 2021). The mismatch in thermal expansion between mineral grains begins to be substantial, leading to the development of numerous microcracks along with the mineral particles. At the same time, there is a significant loss of bound water within the rock, destroying some of the mineral crystal structures. All these factors lead to a reduction in the strength of the rock. However, it can be found that some sandstones with a high content of clay minerals still show a significant increase in compressive strength. The main factor causing this phenomenon are sintering, cementation, and fusing between clay minerals inside the sandstone under the action of high temperature (Ersoy et al. 2021; Xu et al. 2017), which can increase the compactness of the sandstone.

In the third stage (400–800 °C), most sandstone specimens show a rapid decrease in tensile and compressive strength except for sandstones with a high clay mineral content. At this stage, the primary damage source is the mismatch in thermal expansion between the mineral grains, leading to the generation of some grain boundary microcracks. On the other hand, the α - β phase transition of quartz at 573 °C also reduces rock strength.

In the fourth stage (800–1000 °C), when the temperature rises above 800 °C, the diffraction peaks of muscovite and chlorite disappear in the XRD test results (Fig. 17a), which indicates that some rock-forming minerals have decomposed. At this stage, the mechanical strength of all sandstones decreases significantly.

Unlike the complex variation of rock strength with temperature, the P-wave velocity of sandstones only increases

Table 2 Quantitative results of element mass fraction

Mass%	C	O	Na	Al	Si	Au	Total
001	16.68	60.29	2.54	3.23	7.93	9.33	100.00
002	4.23	53.45	0.61	1.44	29.81	10.46	100.00

Table 3 Summary of the experimental studies on sandstone after exposure to different temperatures

No	Sandstone type (region)	Dominant minerals	Heating conditions			Investigated properties		References
			Max temp. (°C)	Heating rate (°C/min)	Holding time (h)	Cooling method		
1	Barakar sandstone (Jharkhand area, India)	Quartz (64%), feldspar (12%), muscovite (4.19%), clay minerals (5%), fine fragments (0.5%)	800	5	24	Furnace	Surface colour, mass loss, wave velocity, porosity, UCS, BTS, Young's modulus	Tripathi et al. (2021)
2	Qinling sandstone (Qinling mountain, China)	Quartz, calcite	1000	10	2	Furnace	Mass loss, Wave velocity, UCS, BTS	Chen et al. (2013)
3	Cottaer sandstone (Cottaer, Germany)	Quartz, kaolinitic, illite	900	H ₁ ^a	6	Air-cooled	UCS, BTS	Hajpál and Török (1998)
4	Donzdorfer sandstone (Donzdorfer, Germany)	Quartz, ferrigenous clayed	900	H ₁ ^a	6	Air-cooled	UCS, BTS	Hajpál and Török (1998)
5	Maulbronner sandstone (Maulbronner, Germany)	Quartz, clayed	900	H ₁ ^a	6	Air-cooled	UCS, BTS	Hajpál and Török (1998)
6	Pliezhausener sandstone (Pliezhausener, Germany)	Quartz, dolomitic	900	H ₁ ^a	6	Air-cooled	UCS, BTS	Hajpál and Török (1998)
7	Ganzhou sandstone (Jiangxi Province, China)	Quartz, feldspar, calcite, clay minerals (small amount)	1000	8	5	Air-cooled	Surface colour, mass loss, porosity, wave velocity, thermal conductivity, BTS	Huang et al. (2021)
8	Fushun sandstone (Liaoning Province, China)	Quartz, muscovite, nacrite, albite	900	5	2	5 °C/min	Porosity, permeability, UCS, peak strain	Li et al. (2020)
9	Jodhpur sandstone (Rajasthan, India)	Quartz (80.2%), dickite (7.3%), kaolinite (6.8%), calcite (5.4%), spinel (0.4%)	900	5	3	5 °C/min	UCS, BTS, Poisson's ratio, Young's modulus, failure strain	Mahanta et al. (2020)
10	Hawkesbury sandstone (Gosford, Australia)	Quartz (85%), kaolinite (7%), muscovite (3%), goethite (2%), smectite (2%), anatase (1%)	950	5	2	Furnace	UCS, elastic modulus	Ranjith et al. (2012)
11	Hawkesbury sandstone (Gosford, Australia)	Quartz (74%), kaolinite (12%), siderite (7%), barite (4%), calcite (2%), mica (<1%), smectite (<1%)	1000	5	24	Air-cooled	UCS, Young's modulus, Poisson's ratio	Rathnaweera et al. (2018)
12	Dholpur sandstone (Rajasthan, India)	Quartz, feldspar	1000	5	120	Air-cooled	UCS, BTS, friction angle, cohesion, Poisson's ratio, Young's modulus	Sirdesai et al. (2017)
13	Jiaozuo sandstone (Henan Province, China)	Quartz, feldspar, mica	900	10	4	Furnace	Wave velocity, elastic modulus, peak strain, UCS	Su et al. (2008)
14	Rizhao sandstone (Shandong Province, China)	Quartz, feldspar, calcite, haematite, clay minerals	1000	5	2	Furnace	UCS, BTS, K _{IC} , TCS, permeability, elastic modulus, Poisson's ratio	Yang et al. (2020)

Table 3 (continued)

No	Sandstone type (region)	Dominant minerals	Heating conditions			Investigated properties	References	
			Max temp. (°C)	Heating rate (°C/min)	Holding time (h)			Cooling method
15	Linyi sandstone (Shandong Province, China)	Quartz, dolomite/ankerite, kaolinite, feldspar, biotite, haematite/magnetite	900	5	1	5 °C/min	Porosity, resistivity, UCS	Zhang et al. (2016)
16	Linyi sandstone (Shandong Province, China)	Quartz (78%), albite (10%), aluminosilicate (9%), calcite (3%)	1300	10	1	Furnace	Porosity, BTS	Zhang et al. (2021)
17	Changsha sandstone (Hunan Province, China)	Quartz (65.68%), feldspar (21.35%), montmorillonite (4.58%), muscovite (3.67%), chlorite (4.72%)	1200	3	2	Furnace	Surface colour, density, wave velocity, porosity, UCS, BTS, brittleness index, mineralogical analysis, elastic modulus	Current study

^aH₁ heating procedure took 1 h to reach the required temperature

marginally up to 200 °C and then decreases steadily above 200 °C, as shown in Fig. 21c. The main reason for this discrepancy is that the propagation of ultrasound is mainly influenced by the porosity of the rock. The elastic modulus of sandstone shows a significant decrease at around 500 °C, which is in good agreement with the variation in the brittleness index of sandstone obtained in this study, which also indicates that the high-temperature treatment reduces the sandstone’s elasticity and brittleness.

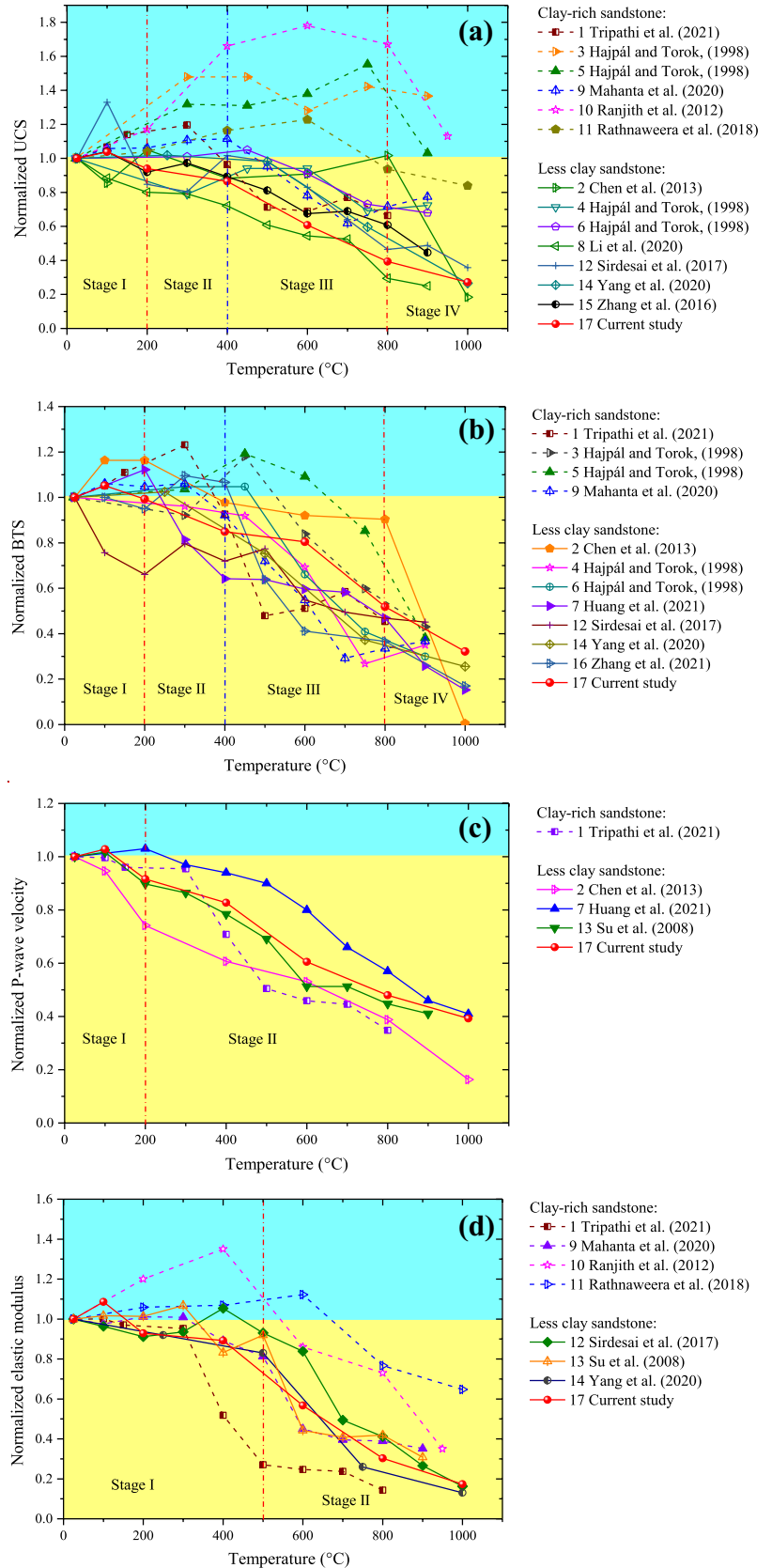
Engineering practice values

In many rock projects, such as the recovery of geothermal energy, underground coal gasification (UCG), deep disposal of highly radioactive nuclear waste, and geological storage of carbon dioxide, the problems of thermal cracking, strength, deformation, and stability of rocks under high temperature are involved. Quantifying the effects of high-temperature treatment on the physical–mechanical, mineralogical and microstructural properties of rocks is therefore of great importance to ensure the structural safety and long-term stability of rock mass projects. This paper uses an integrated technology approach to investigate the underlying mechanisms of temperature influence on rock strength. The research has yielded many important findings that can be used to guide engineering practice.

As we know, the underground coal gasification and the storage of nuclear waste both have a gradient effect on the heat transfer to the surrounding rock mass. This paper shows that the effect of high temperature on the macro-mechanical properties of rock has apparent stages. Before 100° C, the high temperature will not damage the surrounding rock but can strengthen the rock engineering. Significantly, the mechanical properties of sandstones containing more clay minerals are more likely to be strengthened by temperature. When the temperature exceeds 800 °C, the strength of sandstone can be reduced by 80%, which also indicates that the rock has lost its bearing capacity. Under different temperature conditions, the chemical changes of rock-forming minerals lead to significant damage to the rock. We can take these particular temperature points as the engineering warning temperature.

On the other hand, the ground temperature is an important external factor affecting rock engineering. The temperature of the rock gradually rises with increasing depth of burial, especially in certain areas where faults and geological movements are active, and the temperature gradient ranges even to 30–200 °C/km (Cai and Brown 2017). During deep mining, excavation and ventilation cause the high-temperature rock mass to cool gradually. The physical and mechanical parameters of the rock after high temperatures are crucial for designing the mining pillar size in the goaf. Moreover, deep rock engineering may often encounter

Fig. 21 Comparisons with existing literature. **a** Normalized UCS vs. temperature; **b** normalized BTS vs. temperature; **c** normalized P-wave velocity vs. temperature; **d** normalized elastic modulus vs. temperature



sudden high-temperature events, such as underground coal gasification (Roddy and Younger 2010), mine gas explosion (Tripathi et al. 2021), and building or tunnel fires (Das et al. 2017). The post-disaster reconstruction, repair, reinforcement, and safety assessment of the deep rock engineering also need to consider the changes in the properties of the rock after high temperatures.

Conclusions

1. The physical and mechanical parameters of tested sandstone show different degrees of strengthening until a temperature of 100 °C caused mainly by the evaporation of free water and the thermal expansion of mineral particles inside the sandstone. Beyond 100 °C, the physico-mechanical properties of sandstone experience significant weakening with increasing temperature. Mass loss and porosity show a continuous growing trend with increasing temperature, while P-wave velocity, tensile and compressive strength, and elastic modulus exhibit a decline.
2. NMR testing results show that heat treatment has a great influence on the pore structure characteristics of sandstone. The porosity increases with the increase of temperature resulting in a linear relationship between rock porosity and compressive as well as tensile strength. When the temperature rises up to 400 °C, green aggregation area appears in the NMR images, indicating the extension and coalescence of microcracks, which leads to an increase in the proportion of macropores. Extremely high temperatures like 1200 °C lead to melting and recrystallization of the rock, resulting in qualitative changes in its pore structure.
3. Chemical reaction and thermal expansion of mineral particles due to high temperature are the two main factors affecting changes of the fabric of the sandstone. Differential thermal analysis (DTA) shows that the α - β phase transition of quartz minerals occurs at the temperature of 573.4 °C. Between 400 and 600 °C, more transgranular microcracks are observed by using optical microscope and scanning electron microscopy (SEM). When the temperature exceeds 600 °C, the size of crystal particles show a downward trend, which also proves that the α - β phase transition is an important factor to induce microcracks (fragmentation).
4. The brittle index (ration of tensile to compressive strength) exhibits a sharp decline in the temperature range between 400 and 600 °C. When the temperature rises to 600–800 °C, slip separation and dimples occur in the interior of the rock, which are the two most common morphological features for ductile rock fractures, indicating that high temperature treatment makes plastic deformations of the sandstone more obvious.

Funding This work was supported by the National Natural Science Foundation of China (41972283, 11972378), the National Key Scientific Instrument and Equipment Development Project of China (51927808), the Hunan Provincial Innovation Foundation for Post-graduates of China (CX2018B066), and the State Scholarship Fund from the China Scholarship Council (201906370133).

Data availability All data in the text are available through the corresponding author.

Declarations

Conflict of interest The authors declare no competing interests.

References

- Altindag R (2010) Assessment of some brittleness indexes in rock-drilling efficiency. *Rock Mech Rock Eng* 43(3):361–370
- Aydin A (2014) Upgraded ISRM suggested method for determining sound velocity by ultrasonic pulse transmission technique. *Rock Mech Rock Eng* 47:255–259
- Bieniawski ZT, Hawkes I (1978) Suggested methods for determining tensile strength of rock materials. *Int J Rock Mech Min Sci* 15(15):99–103
- Braun P, Ghabezloo S, Delage P, Sulem J, Conil N (2019) Determination of multiple thermo-hydro-mechanical rock properties in a single transient experiment: application to shales. *Rock Mech Rock Eng* 52(7):2023–2038
- Brotóns V, Tomás R, Ivorra S, Alarcón JC (2013) Temperature influence on the physical and mechanical properties of a porous rock: San Julian's calcarenite. *Eng Geol* 167:117–127
- Cai MF, Brown ET (2017) Challenges in the mining and utilization of deep mineral resources. *Engineering* 3(4):432–433
- Chakrabarti B, Yates T, Lewry A (1996) Effect of fire damage on natural stonework in buildings. *Constr Build Mater* 10(7):539–544
- Chen TF, Xu JY, Liu S, Zhi LP (2013) Experimental study on ultrasonic and mechanical properties of sandstone influenced by water-saturation and high temperature. *Chin J Undergr Sp Eng* 9(6):1236–1241
- Chen YL, Wang SR, Ni J, Azzam R, Fernández-steeger TM (2017) An experimental study of the mechanical properties of granite after high temperature exposure based on mineral characteristics. *Eng Geol* 220:234–242
- Coates GR, Xiao L, Prammer MG (1999) *NMR logging: principles and applications*. Gulf Professional Publishing, Oxford
- Das R, Sirdesai N, Singh T (2017) Analysis of deformational behavior of circular underground opening in soft ground using three-dimensional physical model. 51st US Rock Mechanics/Geomechanics Symposium, San Francisco, California, USA. American Rock Mechanics Association
- Ersoy H, Karahan M, Kolaylı H, Sünnetçi MO (2021) Influence of mineralogical and micro-structural changes on the physical and strength properties of post-thermal-treatment clayey rocks. *Rock Mech Rock Eng* 54:679–694
- Fredrich JT, Wong TF (1986) Micromechanics of thermally induced cracking in three crustal rocks. *J Geophys Res Solid Earth* 91(B12):12743–12764
- Frosch GP, Tillich JE, Haselmeier R, Holz M, Althaus E (2000) Probing the pore space of geothermal reservoir sandstones by nuclear magnetic resonance. *Geothermics* 29:671–687
- Funatsu T, Seto M, Shimada H, Matsui K, Kuruppu M (2004) Combined effects of increasing temperature and confining pressure on the fracture toughness of clay bearing rocks. *Int J Rock Mech Min Sci* 41(6):927–938

- Gautam PK, Verma AK, Maheshwar S, Singh TN (2016) Thermo-mechanical analysis of different types of sandstone at elevated temperature. *Rock Mech Rock Eng* 49(5):1985–1993
- Glover PWJ, Baud P, Darot M, Meredith PG, Boon SA, LeRavalec M, Zoussi S, Reuschlé T (1995) α/β phase transition in quartz monitored using acoustic emissions. *Geophys J Roy Astron Soc* 120(3):775–782
- Griffiths L, Lengliné O, Heap MJ, Baud P, Schmittbuhl J (2018) Thermal cracking in westerly granite monitored using direct wave velocity, coda wave interferometry, and acoustic emissions. *J Geophys Res Solid Earth* 123(3):2246–2261
- Hajpál M (2002) Changes in sandstones of historical monuments exposed to fire or high temperature. *Fire Technol* 38(4):373–382
- Hajpál M, Török Á (1998) Petrophysical and mineralogical studies of burnt sandstones. Proceedings 2nd international PhD Symposium, Budapest, pp 476–485
- Hajpál M, Török Á (2004) Mineralogical and colour changes of quartz sandstones by heat. *Environ Geol* 46(3–4):311–322
- He X, Chen W, Nie B, Mitri H (2011) Electromagnetic emission theory and its application to dynamic phenomena in coal-rock. *Int J Rock Mech Min Sci* 48(8):1352–1358
- Heap MJ, Lavallée Y, Laumann A, Hess KU, Meredith PG, Dingwell DB (2012) How tough is tuff in the event of fire? *Geology* 40(4):311–314
- Huang Z, Zeng W, Gu QX, Wu Y, Zhong W, Zhao K (2021) Investigations of variations in physical and mechanical properties of granite, sandstone, and marble after temperature and acid solution treatments. *Constr Build Mater* 307:124943
- Jin PH, Hu YQ, Shao JX et al (2020) Influence of temperature on the structure of pore–fracture of sandstone. *Rock Mech Rock Eng* 53:1–12
- Karunadasa KSP, Manoratne CH, Pitawala HMTGA, Rajapakse RMG (2018) The composition, unit cell parameters and micro-structure of quartz during phase transformation from α to β as examined by in-situ high-temperature X-ray powder diffraction. *J Phys Chem Solids* 117:131–138
- Li XB, Weng L, Xie XF, Wu QH (2015) Study on the degradation of hard rock with a pre-existing opening under static-dynamic loadings using nuclear magnetic resonance technique. *Chin J Rock Mech Eng* 34:1985–1993
- Li JL, Zhou KP, Liu WJ, Deng HW (2016) NMR research on deterioration characteristics of microscopic structure of sandstones in freeze–thaw cycles. *T Nonferrous Metal Soc* 26:2997–3003
- Li BY, Ju F, Xiao M, Ning P (2018) Thermal stability of granite for high temperature thermal energy storage in concentrating solar power plants. *Appl Therm Eng* 138:409–416
- Li M, Wang DM, Shao ZL (2020) Experimental study on changes of pore structure and mechanical properties of sandstone after high-temperature treatment using nuclear magnetic resonance. *Eng Geol* 275:105739
- Lider MC, Yurtseven H (2018) Correlations between the resonant frequency shifts and the thermodynamic quantities for the α - β transition in quartz. *J Mol Struct* 1159:1–4
- Lin Q, Ge WC, Ma R, Sun DY, Wu FY, Yun SH (1999) Experimental research on water loss melting of crustal rocks. *J Changchun Univ Sci Technol* 29(3):209–214
- Liu S, Xu JY (2015) An experimental study on the physico-mechanical properties of two post-high-temperature rocks. *Eng Geol* 185:63–70
- Liu S, Zhang S, Chen F, Wang CH, Liu MY (2014) Variation of coal permeability under dehydrating and heating: a case study of ulanqab lignite for underground coal gasification. *Energ Fuel* 28(11):6869–6876
- Liu XF, Zhang CL, Yuan SY, Fityus S, Sloan SW, Buzzi O (2016) Effect of high temperature on mineralogy, microstructure, shear stiffness and tensile strength of two Australian mudstones. *Rock Mech Rock Eng* 49(9):3513–3524
- Liu QS, Qian ZC, Wu ZJ (2019) Micro/macro physical and mechanical variation of red sandstone subjected to cyclic heating and cooling: an experimental study. *Bull Eng Geol Environ* 78(3):1485–1499
- Lü C, Sun Q, Zhang WQ, Geng JS, Qi YM, Lu LL (2017) The effect of high temperature on tensile strength of sandstone. *Appl Therm Eng* 111:573–579
- Ma L, Zhang Y (2019) An experimental study on infrared radiation characteristics of sandstone samples under uniaxial loading. *Rock Mech Rock Eng* 52:3493–3500
- Mahanta B, Singh TN, Ranjith PG (2016) Influence of thermal treatment on mode I fracture toughness of certain Indian rocks. *Eng Geol* 210:103–114
- Mahanta B, Ranjith PG, Vishala V, Singh TN (2020) Temperature-induced deformational responses and microstructural alteration of sandstone. *J Petrol Sci Eng* 192:107239
- Meng QB, Wang CK, Liu JF, Zhang MW, Lu MM, Wu Y (2020) Physical and micro-structural characteristics of limestone after high temperature exposure. *Bull Eng Geol Environ* 79:1259–1274
- Mollo S, Vinciguerra S, Iezzi G, Iarocci A, Scarlato P, Heap MJ, Dingwell DB (2011) Volcanic edifice weakening via devolatilization reactions. *Geophys J Int* 186(3):1073–1077
- Nasseri MHB, Tatone BSA, Grasselli G, Young RP (2009) Fracture toughness and fracture roughness interrelationship in thermally treated westerly granite. *Pure Appl Geophys* 166(5–7):801–822
- Ranjith PG, Daniel RV, Bai JC, Samintha APM (2012) Transformation plasticity and the effect of temperature on the mechanical behaviour of Hawkesbury sandstone at atmospheric pressure. *Eng Geol* 151:120–127
- Rao QH, Wang Z, Xie HF, Xie Q (2007) Experimental study of mechanical properties of sandstone at high temperature. *J Cent South Univ Technol* 14:478–483
- Rathnaweera TD, Ranjith PG, Gu X, Perera MSA, Kumari WGP, Wanniarachchi WAM, Haque A, Li JC (2018) Experimental investigation of thermomechanical behaviour of clay-rich sandstone at extreme temperatures followed by cooling treatments. *Int J Rock Mech Min Sci* 107:208–223
- Roddy DJ, Younger PL (2010) Underground coal gasification with CCS: a pathway to decarbonising industry. *Energ Environ Sci* 3(4):400–407
- Rong G, Peng J, Cai M, Yao MD, Zhou CB, Sha S (2018) Experimental investigation of thermal cycling effect on physical and mechanical properties of bedrocks in geothermal fields. *Appl Therm Eng* 141:174–185
- Shafiei A, Dusseault MB (2013) Geomechanics of thermal viscous oil production in sandstones. *J Petrol Sci Eng* 103:121–139
- Shen YJ, Hou X, Yuan JQ, Xu ZH, Hao JS, Gu LJ, Liu ZY (2020) Thermal deterioration of high-temperature granite after cooling shock: multiple-identification and damage mechanism. *Bull Eng Geol Environ* 79:5385–5398
- Sirdesai NN, Singh TN, Ranjith PG (2017) Thermal alterations in the poro-mechanical characteristic of an Indian sandstone: a comparative study. *Eng Geol* 226:208–220
- Sirdesai NN, Mahanta B, Ranjith PG, Singh TN (2019) Effects of thermal treatment on physico-morphological properties of Indian fine-grained sandstone. *Bull Eng Geol Environ* 78:883–897
- Su CD, Guo WB, Li XS (2008) Experimental research on mechanical properties of coarse sandstone after high temperatures. *Chin J Rock Mech Eng* 6(27):1162–1170
- Tang ZQ, Zhai C, Zou QL, Qin L (2016) Changes to coal pores and fracture development by ultrasonic wave excitation using nuclear magnetic resonance. *Fuel* 186:571–578
- Tian H, Kempk T, Xu NX, Ziegler M (2012) Physical properties of sandstones after high temperature treatment. *Rock Mech Rock Eng* 45:1113–1117

- Tian H, Ziegler M, Kempka T (2014) Physical and mechanical behavior of claystone exposed to temperatures up to 1000 °C. *Int J Rock Mech Min Sci* 70:144–153
- Tripathi A, Gupta N, Kumar A, Singh AK, Mohanty SP, Rai N, Pain A (2021) Effects of elevated temperatures on the microstructural, physico-mechanical and elastic properties of Barakar sandstone: a study from one of the world's largest underground coalmine fire region, Jharia, India. *Rock Mech Rock Eng* 54:1293–1314
- Vostretsov AG, Krivetsky AV, Yakovitskaya GE (2010) Detection of fracture stage change in rocks using nonstationary Poisson pulse flow of electromagnetic emission. *Int J Rock Mech Min* 47(4):698–701
- Wadsworth FB, Heap MJ, Dingwell DB (2016) Friendly fire: engineering a fort wall in the Iron Age. *J Archaeol Sci* 67:7–13
- Wang P, Yin T, Li X, Zhang S, Bai L (2019) Dynamic properties of thermally treated granite subjected to cyclic impact loading. *Rock Mech Rock Eng* 52(4):991–1010
- Westphal H, Surholt I, Kiesel C, Thern HF, Kruspe T (2005) NMR measurements in carbonate rocks: problems and an approach to a solution. *Pure Appl Geophys* 162:549–570
- Wolters F, Emmerich K (2007) Thermal reactions of smectites—relation of dehydroxylation temperature to octahedral structure. *Thermochim Acta* 462(1–2):80–88
- Wong LNY, Zhang Y, Wu Z (2020) Rock strengthening or weakening upon heating in the mild temperature range? *Eng Geol* 272:105619
- Wong LNY, Guo TY, Wu Z, Xiao XY (2021) How do thermally induced microcracks alter microcracking mechanisms in Hong Kong granite? *Eng Geol* 292:106268
- Wood SH, Kaewsomwang P (2018) Geologic framework of the Fang Hot Springs area with emphasis on structure, hydrology, and geothermal development, Chiang Mai Province, northern Thailand. *Geotherm Energy* 6(1):1–51
- Wu XP, Zhang HF, Guo JG, Hu C, Liu XY (1999) MAS NMR spectra of montmorillonite and its thermal treatment products. *J Inorg Mater* 14(4):580–586
- Xie KN, Jiang DY, Sun ZG, Chen J, Zhang WG, Jiang X (2018) NMR, MRI and AE statistical study of damage due to a low number of wetting–drying cycles in sandstone from the three gorges reservoir area. *Rock Mech Rock Eng* 51(11):3625–3634
- Xu XL, Gao F, Zhang ZZ (2017) Thermo-mechanical coupling damage constitutive model of rock based on the Hoek-Brown strength criterion. *Int J Damage Mech* 27:1213–1230
- Xue DJ, Zhou HW, Liu YT, Deng LS, Zhang L (2018) Study of drainage and percolation of Nitrogen–water flooding in tight coal by NMR imaging. *Rock Mech Rock Eng* 51:3421–3437
- Yang S, Hu B, Tian W (2020) Effect of high temperature damage on triaxial mechanical failure behavior of sandstone specimens containing a single fissure. *Eng Fract Mech* 233:107066
- Yao YB, Liu DM, Che Y, Tang DZ, Tang SH, Huang WH (2010) Petrophysical characterization of coals by low-field nuclear magnetic resonance (NMR). *Fuel* 89(7):1371–1380
- Yi W, Rao QH, Li Z, Shen QQ (2019) A new measurement method of crack propagation rate for brittle rock under THMC coupling condition. *T Nonferrous Metal Soc* 29:1728–1736
- Zhang WQ, Sun Q, Hao SQ, Yang L (2016) Experimental study of the effect of thermal damage on resistivity and mechanical properties of sandstone. *Acta Geodyn Geomater* 13:185–192
- Zhang YL, Sun Q, Geng JS (2017) Microstructural characterization of limestone exposed to heat with XRD, SEM and TG-DSC. *Mater Charact* 134:285–295
- Zhang WQ, Sun Q, Zhu YM, Guo WH (2019) Experimental study on response characteristics of micro–macroscopic performance of red sandstone after high-temperature treatment. *J Therm Anal Calorim* 136:1935–1945
- Zhang H, Sun Q, Jia H, Dong Z, Luo T (2021) Effects of high-temperature thermal treatment on the porosity of red sandstone: an NMR analysis. *Acta Geophys* 7:113–124
- Zhao YX, Song HH, Liu SM, Zhang CG, Dou LM, Cao A (2019) Mechanical anisotropy of coal with considerations of realistic microstructures and external loading directions. *Int J Rock Mech Min Sci* 116:111–121
- Zhou YX, Xia KW, Li XB, Li HB, Ma GW, Zhao J, Zhou ZL, Dai F (2012) Suggested methods for determining the dynamic strength parameters and mode-I fracture toughness of rock materials. *Int J Rock Mech Min Sci* 49(1):105–112
- Zuo J, Li Y, Zhang X, Zhao Z, Wang TZ (2018) The effects of thermal treatments on the subcritical crack growth of Pingdingshan sandstone at elevated high temperatures. *Rock Mech Rock Eng* 51(11):3439–3454

Springer Nature or its licensor (e.g. a society or other partner) holds exclusive rights to this article under a publishing agreement with the author(s) or other rightsholder(s); author self-archiving of the accepted manuscript version of this article is solely governed by the terms of such publishing agreement and applicable law.